Journal of Environmental Chemical Engineering 14 (2026) 122311

Contents lists available at ScienceDirect

Journal of Environmental Chemical Engineering

journal homepage: www.elsevier.com/locate/jece

# From pulp to aromatic products – Kinetic modeling of hydrothermal lignin depolymerization

Maximilian Wörner, Bruno Lacerda de Oliveira Campos, Ursel Hornung *, Nicolaus Dahmen

*Karlsruhe Institute of Technology (KIT), Institute of Catalysis Research and Development (IKFT), Hermann-von-Helmholtz-Platz 1, Eggenstein-Leopoldshafen 76344, Germany*

ARTICLE INFO

*Keywords:*
Lignin
Biomass valorization
Hydrothermal liquefaction
Black liquor
Kinetic model
Biorefinery
Bio-based chemicals

ABSTRACT

Lignin is a promising renewable feedstock for producing aromatic platform chemicals due to its high content of aromatic structures linked by various chemical bonds. In the pulp industry, lignin occurs in large quantities dissolved in the black liquor providing a possible feedstock for depolymerization into interesting aromatic monomers. This work studied the lignin depolymerization process under hydrothermal conditions ($T_R$ = 300 – 350 °C, $t_R$ = 0 – 30 min, $p$ = 200 bar), using a black liquor based on eucalyptus wood as feedstock. The aim was to understand the main reaction pathways of the lignin depolymerization. Experiments were performed in batch micro autoclaves and the product phases were separated and characterized. The work focused on the principal aromatic monomers, mainly different forms of catechol. Based on the experimental results a reaction scheme was set up consisting of the aromatic monomers, lumped groups like oligomers, and gaseous compounds. A kinetic model was developed, parametrized, and trained, providing adequate results. The calculated kinetic parameters and the developed reaction scheme were compared with data from literature. In accordance with our model, the main pathway from lignin to methylated catechols is via 3-methoxycatechol and catechol. Finally, experimental results of hydrothermal liquefaction (HTL) with softwood black liquor were compared with the calculated yield curves and showed limited deviations. Hence, this implies that the model, with minor adjustments, can be used for the HTL of softwood black liquor as the dissolved salts presumably have a significantly greater influence than the type of wood.

## 1. Introduction

The impact of the climate change on our planet is steadily increasing [1]. To mitigate this impact, humankind is required to act. This urgent need prompted 195 countries to set up the Paris Climate Agreement of 2015 with the aim of keeping global warming below two degrees Celsius in order to avoid potentially irreversible tipping points being reached in our environment [2]. The most effective mechanism is viewed as the reduction of greenhouse gases (GHG), of which carbon dioxide (CO2) is the most prominent. However, the big challenge is the fact that energy consumption continues to rise [3], the primary contributor to CO2 emissions, since most of those energy resources are based on fossil fuels. For example, there has been an increase of approximately 2% between 2022 to 2023 in worldwide primary energy consumption, with the total in 2023 reaching 619.63 EJ [4]. To achieve an enduring reduction in CO2 emissions inevitably entails a reduction in the use of fossil resources such as coal, crude oil and natural gas. This in turn raises probing questions, not only for the energy sector but also for the entire chemicals industry. A reduction specifically of crude oil will ultimately lead to shortages in the supply chains of these chemicals. A cogent example here are the aromatic compounds. These play an important role in the chemicals industry and, consequently, across a broad cross section of the needs of modern life [5]. Today, the most important group of aromatics for the synthesis routes is known as the BTX group, an acronym for benzene, toluene and xylene. These are produced in large quantities in the crude oil refining process. The global production of BTX was estimated at 128 MT in 2022 [6]. The biggest share is obtained in the catalytic cracking or steam cracking of different naphtha fractions [7]. The main route for the production of phenol and its derivatives involves the use of benzene as the main feedstock in the prominent Cumene process

* Corresponding author.
*E-mail addresses:* maximilian.woerner@kit.edu (M. Wörner), bruno.campos@kit.edu (B. Lacerda de Oliveira Campos), ursel.hornung@kit.edu (U. Hornung), nicolaus.dahmen@kit.edu (N. Dahmen).

https://doi.org/10.1016/j.jece.2026.122311
Received 19 December 2025; Received in revised form 17 February 2026; Accepted 19 March 2026
Available online 20 March 2026

[8]. Approximately, 11 MT of phenol were produced globally in 2024 with further increases anticipated over the next few yearsi [9]. Most of the other phenolic compounds such as catechol, the substance upon which this study focuses, are products of synthesis routes involving the use of phenol [10]. The targeted products of this process chain are often specific chemicals that are used in a wide range of applications, from agriculture to medicine.

The possible reduction in the usage of crude oil drives a parallel need to provide alternatives for the supply of aromatic compounds. Not only do new potential renewable feedstocks have to be found, but also new process routes need to be developed. Different promising feedstocks and processes are under research or already under development. Examples include the production of aromatics from bio-based methanol or bio-based furan derivatives [11–15]. However, in both cases several process steps have to be applied to reach the target product. In the methanol to aromatic route (MtA), biomass must first be converted to synthesis gas [16,17] from which methanol can then be produced [18–20]. The same is true of furans, which can be produced using hydrothermal conversion, to cite just one example [21]. In this case, an additional question arises as to whether it is even worthwhile converting furan derivatives into other platform chemicals, as they themselves already have great potential, especially for the polymer industry [22,23]. The main products of the MtA process are aromatic compounds related to the BTX fraction.

One possible alternative feedstock for the production of aromatics, especially phenolic compounds, is the biopolymer lignin. This would not only help to reduce crude oil usage, it would also produce phenolic aromatics directly, without the need for an extra synthesis route starting from BTX. Lignin occurs naturally in plants and trees and is a part of the lignocellulose. Depending on the degree of lignification, the proportion of lignin integrated into the cell walls varies and provides the stability of the plant or tree [24,25]. Fig. 2 shows a potential segment of a lignin molecule [26]. The high density of aromatic rings is a particularly striking feature. With the exception of fossil materials such as coal, this is not found in any other raw material that is as prevalent in the natural world. In the search for possible new and sustainable sources of aromatics, lignin is therefore a promising solution. By splitting the bonds between the aromatic rings, various phenolic compounds or bio-oil can be produced.

In addition to the interesting characteristics of lignin, there is a second aspect that demonstrates the great potential for valorization. It is produced in large quantities as a by-product in the pulp industry, globally estimated at 50 million tons per year [27]. In the most commonly used process for pulping wood, the Kraft process, the lignocellulose is separated in to its main constituents under alkaline conditions. While the cellulose is further processed for paper and cardboard production, hemicellulose and lignin remain in solution together with the cooking chemicals used, such as sodium sulfide ($Na_2S$) or sodium hydroxide (NaOH). This solution is called black liquor and is thickened in the recovery boiler to allow chemicals to be recycled after the organic remnants, such as lignin have been combusted. However, modern pulp mills generate a large surplus of energy. This energy is typically converted into power and sold [28]. As the price of electricity is generally subject to considerable fluctuations, the material recycling of lignin also holds great economic potential. At the same time, the concept of a biorefinery can be implemented with the involvement of the pulp industry, in which all material and energy flows based on renewable raw materials are used as efficiently and sensibly as possible. The biorefinery based on lignocellulose lends itself very well to this due to the versatility of the feedstock [29–33]. A current example of an existing biorefinery is the Äänekoski bioproduct mill operated by Metsä in Äänekoski, Finland. This plant primarily produces pulp and sawn timber based on wood, as well as a broad portfolio of other products [34]. Other examples of biorefineries based on wood are Lenzing in Austria [35] and the biorefinery of UPM Biochemicals in Leuna, Germany which is currently under construction [36]. There are different processes to depolymerize the lignin molecule, which are depicted in Fig. 2.

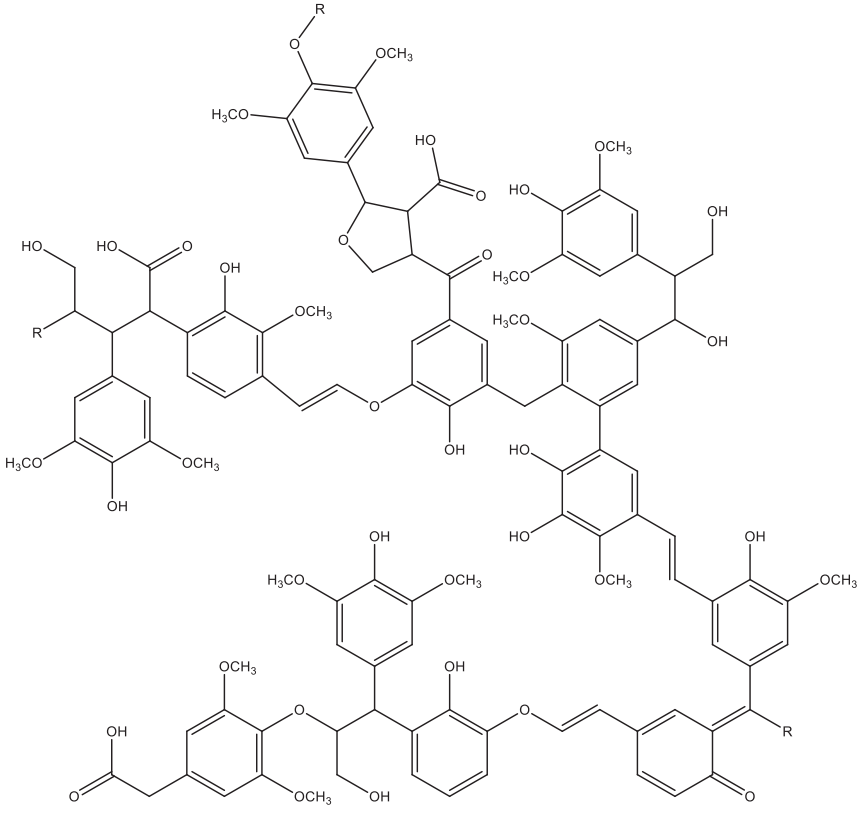


**Fig. 1.** Possible chemical structure of a part of lignin; reproduced with permission from ref. Lange et al. [26]; Copyright 2013 Elsevier.

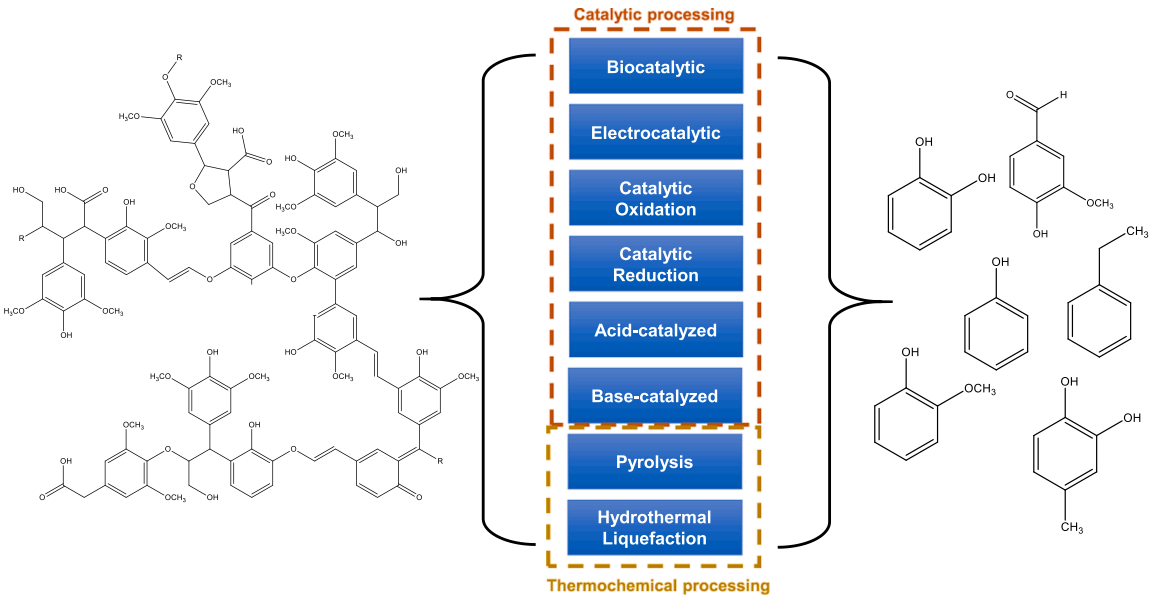


**Fig. 2.** Overview of the described depolymerization processes for lignin depolymerization to aromatics; reproduced with permission from ref. Lange et al. [26]; Copyright 2013 Elsevier.

The processes can be divided into two categories, catalytic and thermochemical. There are biotechnological approaches based on lignin-decomposing enzymes such as laccase [37–39] as well as electrocatalytic processes that depolymerize the lignin molecule through the applied voltage and the electrolyte (homogeneous catalyst) or the electrode (heterogeneous catalyst) [40–42].In addition, there are also numerous chemical catalytic approaches with well-known metal catalysts or acids and bases. These are also able to break down specific bonds in the lignin structure [43–49]. However, the focus for this work is on HTL, a thermochemical process. In HTL, a pressure of $p = 200 – 350$ bar and a temperature in the range of $T = 250 – 400$ °C are typically applied. HTL can process a feedstock with over 90 % water content. In fact, water is necessary for the process as a catalyst, reactant and solvent, as it undergoes drastic changes in properties under conditions close to the critical point of water ($T_c$ = 374 °C, $p_c$ = 221 bar). This leads to an intensification and acceleration of the depolymerization reactions due to higher solubility of non-polar compounds and catalytic effects based on the higher concentration of $H^+$ and $OH^-$ ions [50–52]. This is an advantage compared to pyrolysis, another thermochemical process and one that requires an almost dry feedstock and primarily forces radical-induced cleavage reactions.

For this reason, numerous scientific studies are focusing on gaining a better understanding of the depolymerization of lignin under typical HTL conditions. The aim here is to target specific products more precisely and to elucidate the underlying reaction mechanisms. In many studies, technical lignin is used as the starting material, dissolved in an alkaline solution. Potassium or sodium salts are often used for this, usually in the form of sodium/potassium hydroxides or carbonates (NaOH, KOH, $Na_2CO_3$ or $K_2CO_3$). This is because they can also function as homogeneous catalysts. Different influences on the HTL process were investigated. For example, Belkheiri et al. investigated the influence of the sodium-potassium ratio on the yields of various product phases and on phenolic compounds [53,54]. This investigation revealed that the solids content in the light oil fraction in particular decreased in response to an increasing sodium content, while also increasing significantly in the heavy oil fraction. In the work of Cheng et al. the impact of a different solvent mixture containing water and ethanol was studied [55]. Even a pure organic solvent can be used, which is then correctly called a solvolysis. Forchheim et al. compared in their study the depolymerization of lignin in water and in ethanoll [56,57]. They observed that both approaches resulted in depolymerization, but that the aromatics produced differed due to the reaction of ethanol. Another major challenge in the HTL of lignin is repolymerization. Due to the large number of functional groups of the resulting monomers, there is a high probability of repolymerization. To mitigate this, capping agents such as phenol, boric acid or other substances can be used [54,58–61]. However, this tends to create other products because these capping agents often bind to the functional groups when mitigating repolymerization.

The effect of heterogeneous catalysts on depolymerization has also been investigated in studies. In the work of Forchheim et al., Raney-Nickel was able to achieve an improved yield of phenol, as hydrodeoxygenation was accelerated [62]. However, recovering the heterogeneous catalyst is a challenge. The studies mentioned so far all have in common that they work with extracted lignin or model substances. In order to integrate the HTL as directly as possible into the system, it makes sense to look at the direct use of black liquor (BL). Not many studies of direct HTL of BL have been published thus far. A detailed parametric study was conducted by Harisankar et al., although they did not use liquid BL directly [63]. Instead, they dried the BL to obtain a solid, which was then mixed with water. Direct HTL of BL was carried out by Orebom et al. at temperatures between 340 °C and 410 °C and residence times ranging from 10 to 120 min, focusing primarily on the yields of bio-oil and biochar [64]. However, the BL used in this case was obtained by cooking wood chips using soda pulping, rather than the sulfur-based Kraft process. As a result, the feedstock was sulfur-free, which may affect the depolymerization behavior of lignin.

In order to show how useful the HTL of BL is for the production of aromatics, we have investigated this in detail in a previous study [65]. We were able to show that catechol in particular is the main product among the aromatics, while methylated catechols are also strongly represented. At the same time, we found that the same reactions observable at monomers take place at the oligomers and that a large proportion of the carbon ends up in the solid under the conditions investigated. Overall, these results improved our understanding of the lignin depolymerization reaction network happening in the HTL of BL.

Kinetic modeling is a powerful tool for better understanding the influence of process parameters in the chemical process, and delivers benefits when scaling up and optimizing such a process. Forchheim et al. and Gasson et al. jointly developed a model for solvolysis with ethanol and HTL using water based on extracted lignin as the feedstock [56,57]. In the work of Jayathilake et al. a numerical shrinking-core model was

developed for lignocellulose under HTL conditions [66]. However, only hydrolysis reactions were considered. While this type of depolymerization reaction predominantly takes place in the lower temperature regime, radical reactions such as those that also take place during pyrolysis become dominant at higher temperatures. Yong and Matsumura were able to show this in their kinetic analysis using guaiacol as a model substance [67,68].

Overall, there are only a few models that consistently describe the depolymerization of lignin. And, to the best of our knowledge, there is no model available in literature that was developed for HTL of BL. Therefore, in this work we developed a model based on the experimental data of our previous study [65] This model focuses on the aromatic compounds, especially the methylated ones which are highly prevalent in the investigated temperature range. A model of this kind can be used as the basis for future works in this field and also going to be used for a possible scale-up of HTL processes.

## 2. Material and methods

### 2.1. Experimental part

#### 2.1.1. Feedstock

The black liquor used was produced at the Figueira da Foz pulp mill in Portugal and supplied by the Navigator Company. The species of wood used for the Kraft process is *Eucalyptus globulus*. Accordingly, it belongs to the hardwoods with a distribution of syringyl to guaiacyl groups (S/G) of 70:30 [69]. The black, malodorous liquid has a homogeneous character, indicating that all substances, whether biomass or salts, are dissolved in the strongly alkaline solution. The most important properties are listed in Table 1. Table 2 lists the elemental composition. All yields of the products were calculated based on $w_{BL,\ burnable}$, assuming that the burnable fraction is approximately equal to the organic fraction (see Cardoso et al. [69]). The BL was dried at 105 °C and afterwards burned at 815 °C. Minor differences may arise due to the change in ash composition caused by combustion and the associated oxidation reactions. For the kinetic model we assumed that the burnable fraction consists only lignin to simplify the model even if in reality other wood residues are part of it. Data from Cardoso et al shows that lignin is the most abundant compound of the dried BL with a concentration higher than 40 wt. %, which is a bit lower than our assumed lignin content 57.9 wt. % equal to the measured organic matter content in dried BL.

#### 2.1.2. Batch experiment setup and product separation

All batch experiments were conducted in micro autoclaves made of stainless steel 1.4571(316Ti), manufactured in the institute workshop. These autoclaves have a volume of $V_R = 25$ mL. A specially designed micro-autoclave station was used for opening, filling and closing (see SI Figure S1). It is connected to a nitrogen source to provide an inert atmosphere. After opening, gas samples can be transferred to a gas trap which can be accessed via a septum. The filling level of black liquor is adapted to suit the density of the water at the corresponding reaction temperatures investigated. For all experiments in this study, the fill level of BL was set to $V_L = 15$ mL. This ensures a pressure of approximately 200 bar during the process. The temperatures investigated were $T_R$ = 300 °C, 325 °C and 350 °C, with several holding times $t_R = 0 – 30$ min. In addition to the holding times, a heating time of $t_h = 10$ min in the fluidized sand bath (SBL 2, Techne, Stone, UK) was set beforehand. The temperature during the heating process at 300 and 350 °C was monitored and is shown in the supplementary information (see Figure S2). At the end of the holding time, the autoclaves were quenched in a water bath to prevent subsequent reactions as quickly as possible. The reactors in the micro-autoclave station were then opened and the product phases were separated in accordance with Fig. 3 as described in the previous work [65]. Since no phase separation occurred in the liquid phase after vacuum filtration, a liquid-liquid extraction (LLE) with the non-polar solvent ethyl acetate was necessary. Acidification of the sample with 6M HCl before adding the extraction solvent was essential. This is because phenolic compounds were present predominantly in ionic form due to their strong alkalinity. Consequently, they are readily soluble in water.

**Table 1**
Properties of the BL used in the experiments $w_{BL,\ burnable}$ calculated from the loss on ignition corrected from the dry matter.

| Dry matter $w_{tr}$ | Ash content $w_{ash,\ 815\ °C}$ | Dry matter-based loss on ignition | Raw BL-based burnable matter $w_{BL,\ burnable}$ | Density $\rho_{BL}$ | pH |
|---|---|---|---|---|---|
| 14.5 wt % | 6.1 wt% | 57.9 wt% | 8.4 wt% | 1.0725 kg*L$^{-1}$ | > 12.5 |

**Table 2**
Elemental composition of the dry mass of the BL; analysis performed via elemental analysis (EA) and inductively coupled plasma - optical emission spectrometry (ICP-OES); oxygen calculated via difference, no other element was detected in relevant amounts.

| Element symbol | Mass fraction dry mass BL / wt% |
|---|---|
| C (EA) | 34 ± 0.4 |
| H (EA) | 3.4 ± 0.5 |
| N (EA) | < 0.1 |
| S (EA) | 4.7 ± 0.1 |
| O (Diff.) | 38.8 |
| Na (ICP) | 17.7 ± 0.9 |
| K (ICP) | 1.3 ± 0.06 |
| Sum | 100 |

#### 2.1.3. Analytic procedure

The total organic carbon (TOC) and total inorganic carbon (TIC) concentration in the liquid product phase before LLE was measured using a Dimatoc 2100 (*Dimatec Analysentechnik GmbH*, Essen, Germany). The gas phase was transferred from the gas trap of the microautoclave station to a gas chromatograph (GC 6890, Hewlett-Packard, now Agilent, Santa Clara, CA, USA; columns Hayesep Q, Molsieve 5A, Restek, Bellefonte, PA, USA) using a gas-tight syringe. The samples were injected at 280 °C splitless mode, with 31.77 mL/min Helium as carrier gas flow. The temperature program in the oven started at 60 °C for 1 min, rising to 200 °C at a rate of 20 °C/min. The final temperature was then held for a further 17 min. The quantified compounds were calibrated beforehand with a calibration gas mixture. Various permanent gases and hydrocarbons were quantified using a flame ionization detector and a thermal conductivity detector (see Table S2 in SI). The gases containing carbon also contributed to the C-balance (see SI). To complete the carbon mass balance an elemental analysis (EA) (Vario EL Cube, Elementar Analysentechnik GmbH, Hanau, Germany) was conducted to analyze the dried solid.

The yields for the gases and the solid were calculated with Eq. (1) based on the the gas masses $m_{c,g}$ from equation S4 and the weighted solid phase $m_s$ after drying at 105 °C.

$$Y_i = \frac{m_i}{w_{BL,burnable} \bullet m_{feed}} \quad (1)$$

Gas chromatography–mass spectrometry (GC–MS; GC 6890N coupled with a 5973 MSD, Agilent, Santa Clara, CA, USA) and gas chromatography with flame ionization detection (GC–FID; GC 7820A, Agilent, Santa Clara, CA, USA) were employed for analysis of the organic phase after LLE to quantify the yield of aromatics. In both systems, separations were carried out using an RTX-5 capillary column (30 m × 0.32 mm × 0.5 µm, Restek, Bellefonte, PA, USA). For GC–MS measurements, samples were injected at 280 °C in splitless mode. Helium was used as the carrier gas at a flow rate of 1.5 ml min$^{-1}$. The oven

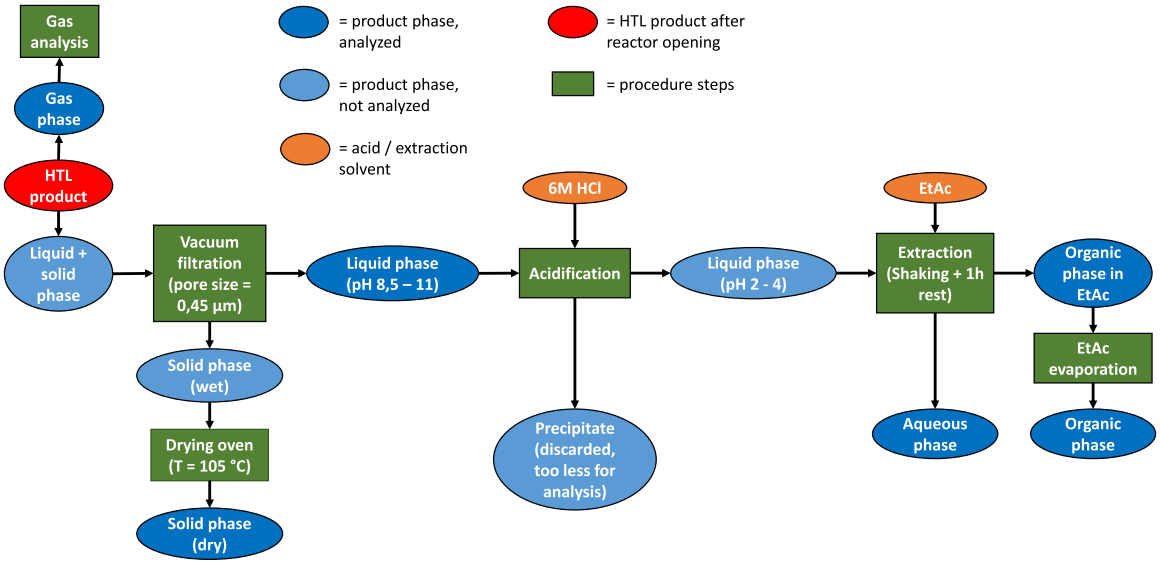


**Fig. 3.** Procedure for HTL product sample separation and analysis with legend, Sample/EtAc ratio for extraction was 1:2.5.

temperature program began at 35 °C with a 5 min hold, followed by heating to 240 °C at 8 °C $min^{-1}$ and a final hold of 10 min. The mass spectrometer was operated in electron impact ionization mode at 70 eV, with the ion source maintained at 230 °C and the quadrupole at 150 °C. A solvent delay of 4.5 min was applied prior to data acquisition, after which spectra were recorded across a mass range of m/z 35–350 at a scan rate of 4.5 scans $s^{-1}$. For GC–FID analysis, samples were injected at 280 °C using a split ratio of 1:50. Helium served as the carrier gas at a flow rate of 1.2 ml $min^{-1}$. The oven temperature was initially held at 50 °C for 2 min, then increased to 190 °C at 8 °C $min^{-1}$, followed by a second ramp to 230 °C at 20 °C $min^{-1}$ and a final hold of 5 min. All quantified compounds were calibrated beforehand with a five-point calibration covering the range of potential peak heights for each compound. Pentadecane was used as an internal standard for the GC-FID. Eq. (2) was used to calculate the concentration of aromatics in the first step. The measured concentration of substance $i(\beta_{i,raw})$ was multiplied by three factors $a - c$, which stand for the total dilution (ethyl acetate and used hydrochloric acid for acidification), the sample volume/EtAc volume ratio and the internal standard (ISTD) factor. The quotient $K_i$ represents the distribution coefficient of the respective compound $i$ in the applied extraction. These were determined in advance and can be found in Table S4 in the SI. The yield $Y_{i,exp}$ could then be calculated using the real concentration $\beta_i$ of a component $i$ in the entire liquid sample (see Eq. (3))

$$\beta_i = \frac{\beta_{i,raw} \bullet a \bullet b \bullet c}{K_i} \left[mg \bullet L^{-1}\right] \quad (2)$$

$$Y_{i,exp} = \frac{\frac{\beta_i}{\rho_{BL}} \bullet m_{liq,prod}}{\frac{w_{BL,burnable}}{\rho_{BL}} \bullet m_{feed}} \left[mg \bullet g^{-1}\right] \quad (3)$$

In order to semi-quantify the possible di- and trimethylcatechols, the ratio of peak area to concentration of the other catechols was determined and transferred to the peak areas of the other substances to be quantified. Quantification by calibrating the GC with the pure di- and trimethylcatechols was not possible as these are not available.

### 2.2. Kinetic modelling

The reaction scheme from Wörner et al. [65] was used as a basis for the kinetic model. The reaction scheme was changed in some parts. A step-by-step methylation of the catechol was added and guaiacol and syringol were eliminated. This was because the concentrations measured were too low. Also, they were only detectable at temperatures below $T_R = 300$ °C. The H+ ion which is needed for demethoxylation was changed to water for sufficient stoichiometry. The model consists of $n = 13$ different components $i$ and, in its initial form, it considers $j = 13$ reaction steps. The model represents the depolymerization of lignin, even if it was not used directly, instead getting dissolved in the black liquor as feedstock. The mass of lignin was set at an equal level to the organic matter in the black liquor $w_{BL,burnable}$ for simplification, since the aim of the model is to describe the lignin depolymerization under the given conditions. The influence of hemicellulose or other organic molecules in the black liquor was not taken into account. The focus of the model is primarily on the reactions involving the aromatic compounds around the catechol. The reaction scheme from the previous work was adjusted at some points (see Fig. 4). The intermediates syringol and guaiacol were not considered because their measured yields in the parameter range investigated were extremely low, making it possible to reduce the level of complexity. What remained was the compound 3-methoxycatechol. This occurs in the previous study as a specific intermediate in hardwood sources and is formed directly from syringol. Since the BL used was also produced from hardwood, this route is the most relevant for catechol production. In addition, the intermediate oligomers (OL_int) were introduced, since it is unlikely that phenolic monomer compounds are formed directly from the lignin molecule. This model does not include the influence of changing water properties nor does it include the potential catalytic effects of the dissolved salts like carbonates, hydroxides and sulfides and produced organo-sulfur products like dimethyl sulfide [70]. The reaction pathways of lignin under hydrothermal conditions itself are not clear yet in relation to state-of-the-art standards. Accordingly, these need to be investigated prior to additional effects like the mentioned ones.

The depolymerization and the reactions on the catechols are driven by hydrolysis and radical-induced reactions. Various studies served as the basis for the different reaction steps, from which hypotheses were derived for this work [67,68,71,72–74]. The reaction of 3-methoxycatechol to catechol (R6) is presumably dominated by radical-driven reactions (see Fig. 5). The overall reaction is proposed in different pathways. In Fig. 5a), methanol is released, especially at lower temperatures, but we were unable to quantify this. Therefore, consideration is given to the combined reactions of methanol formation with methanol reforming to $CO_2$ and $H_2$ as a global side reaction (R10 and R11). Higher temperatures should elevate the methanol reforming anyway, which would support our assumption [75]. In Fig. 5b), a direct radical split in the methoxy group is shown, which we consider to be one of the main pathways. Ionic reactions are also possible, for example a nucleophilic

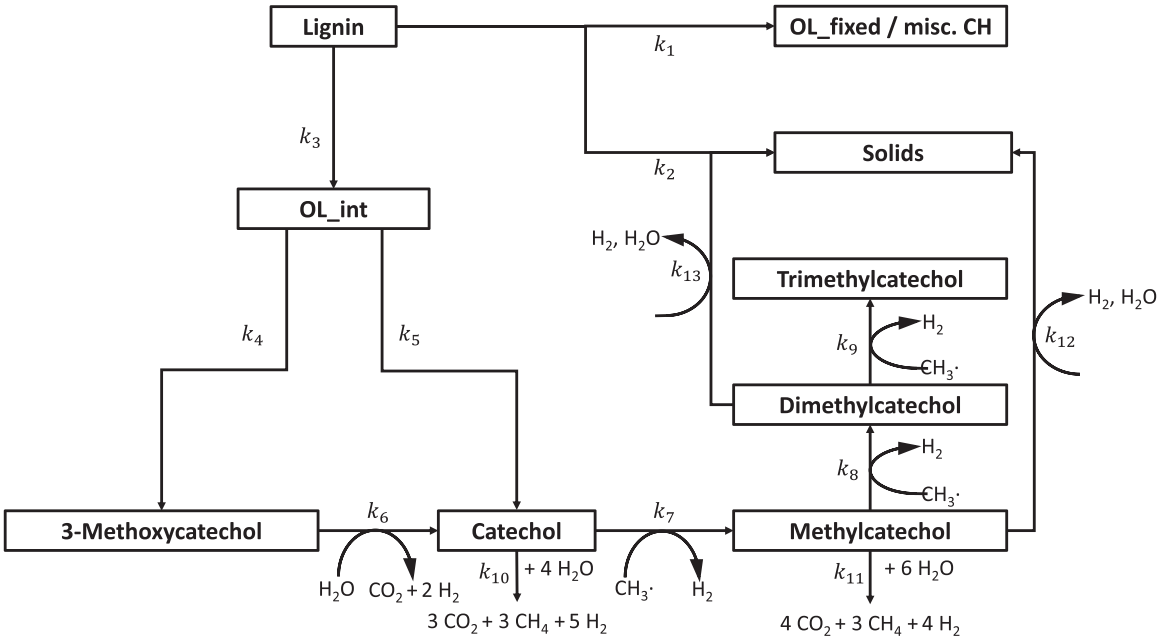


**Fig. 4.** Reaction scheme for the developed kinetic model for lignin depolymerization under hydrothermal conditions with focus on the catechols based on Wörner et al. [65].

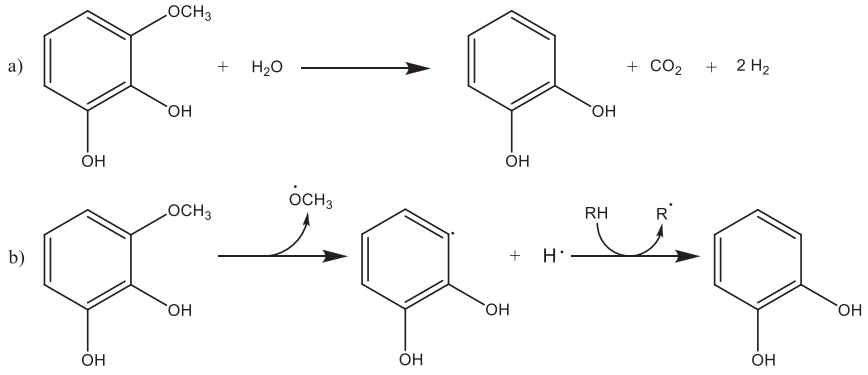


**Fig. 5.** Overview of hypothetical reaction pathways for the step from 3-methoxycatechol to catechol based on observations and studies from Yong and Matsumura [67,68] and Wahyudiono et al. [71,72,76]. a) Reaction considered in the kinetic modeling, with direct conversion of methanol to carbon dioxide and hydrogen; b) Potential direct conversion of 3-methoxycatechol to catechol based on radical forming and interactions. The radical is converted to methanol afterwards, which is directly reformed as mentioned in description for a).

aromatic substitution which can transform the methoxy group into a hydroxy group, which is a common theory for guaiacol to catechol reactions [72]. The following hydrodeoxygenation or hydrolysis reactions can reduce the number of hydroxy groups attached to the ring. Since we could detect pyrogallol (3 hydroxy groups attached) and other aromatics with three oxygen-containing functional groups only in traces compared to 3-Methoxycatechol we assume that the radical reactions are dominant. Fig. 6 illustrates the subsequent methylation of the catechol, probably by methyl radicals. Since radicals and their concentrations cannot be detected during the process, the intermediate oligomers (OL_int) are taken as methyl donors, as the methyl radicals can arise from all alkyl radicals on the molecules.

The subsequent reaction steps are the repolymerization reactions of the molecules, represented in the model by the repolymerization of methylcatechols (R12) and dimethylcatechols (R13), as well as the complete degradation of catechols (R10) and methylcatechols (R11) to gas products, since the yield decrease of aromatics cannot be explained by repolymerization alone. Fixed oligomers (OL_fixed) and other hydrocarbons produced were summarized in a group and calculated using the difference of all yields starting from 100 %. SEC analysis in a previous study shows that there are some larger molecules which are not represented quantitatively in one of the used analysis methods. The same goes for other hydrocarbons in the aqueous phase like alcohols and acids [65]. These are represented with the OL_fixed lump in the model. We assume that $H_2$, $CO_2$, $CH_4$ are only present in the gas phase. The presence of other volatile compounds is negligible, as the carbon mass balance shows. In addition, this model focused primarily on the aromatic compounds in the liquid phase product. Water can be present in the liquid phase as well as in the gas phase. All other compounds are assumed to be present in the liquid phase. Therefore, all reactions were considered to take place only in the liquid phase. All reactions which a part of the kinetic model are listed in Table 3.

The reaction rates ($r_j$) were calculated considering first order reaction in relation to the reactants (see Table 4). Here, $k_j$ is the reaction constant of reaction $j$ ($h^{-1}$) and $\rho_i$ is the mass concentration of species $i$ in the liquid ($kg \cdot m^{-3}$), calculated as follows:

$$\rho_i = \frac{m_{i,liq}}{V_L} \quad [kg \cdot m^{-3}] \tag{4}$$

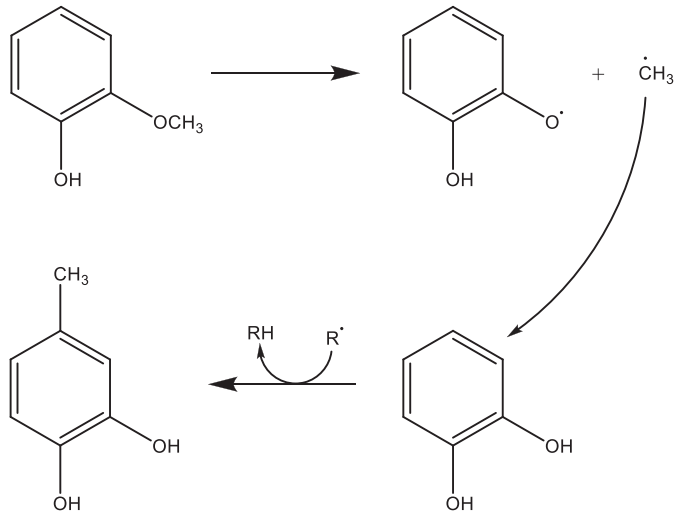


**Fig. 6.** A possible source of methyl radicals from a methoxy group with the following radical driven methylation of a catechol molecule; This reaction step is implemented as R7 and adapted for R8 and R9.

**Table 3**
Overview of all reactions in the kinetic model.

| Reaction N° | Reaction |
|---|---|
| (R1) | Lignin → Oligomers fixed (OL_fixed) /miscellaneous CH |
| (R2) | Lignin → Solids |
| (R3) | Lignin → Intermediate oligomers (OL_int) |
| (R4) | OL_int → 3-Methoxycatechol |
| (R5) | OL_int → Catechol |
| (R6) | 3-Methoxycatechol + $H_2O$ → Catechol + $CO_2$ + 2 $H_2$ |
| (R7) | Catechol + $CH_3$· (from OL_int) → Methylcatechol + $H_2$ |
| (R8) | Methylcatechol + $CH_3$· (from OL_int) → Dimethylcatechol + $H_2$ |
| (R9) | Dimethylcatechol + $CH_3$· (from OL_int) → Trimethylcatechol + $H_2$ |
| (R10) | Catechol + 4 $H_2O$ → 3 $CO_2$ + 3 $CH_4$ + 5 $H_2$ |
| (R11) | Methylcatechol + 6 $H_2O$ → 4 $CO_2$ + 3 $CH_4$ + 4 $H_2$ |
| (R12) | Methylcatechol → Solids + $H_2$ + $H_2O$ |
| (R13) | Dimethylcatechol → Solids + $H_2$ + $H_2O$ |

**Table 4**
Reaction rate equations for all 13 reactions in the kinetic model.

| Reaction rate equation | Reaction N° |
|---|---|
| $r_1 = k_1 \bullet \rho_1$ | (R1) |
| $r_2 = k_2 \bullet \rho_1$ | (R2) |
| $r_3 = k_3 \bullet \rho_1$ | (R3) |
| $r_4 = k_4 \bullet \rho_2$ | (R4) |
| $r_5 = k_5 \bullet \rho_2$ | (R5) |
| $r_6 = k_6 \bullet \rho_3 \bullet \rho_{10}$ | (R6) |
| $r_7 = k_7 \bullet \rho_4 \bullet \rho_2$ | (R7) |
| $r_8 = k_8 \bullet \rho_5 \bullet \rho_2$ | (R8) |
| $r_9 = k_9 \bullet \rho_6 \bullet \rho_2$ | (R9) |
| $r_{10} = k_{10} \bullet \rho_4 \bullet \rho_{10}$ | (R10) |
| $r_{11} = k_{11} \bullet \rho_5 \bullet \rho_{10}$ | (R11) |
| $r_{12} = k_{12} \bullet \rho_5$ | (R12) |
| $r_{13} = k_{13} \bullet \rho_6$ | (R13) |

where $m_{i,liq}$ is the mass of component $i$ in the liquid phase (kg) and $V_L$ is the volume of the liquid set to 15 mL. We used mass concentration since we do not have absolute molar masses for lignin and oligomers.

The reaction constants were calculated using a modified Arrhenius equation (see Eq. (5)): with $T_{ref}$ = 325 °C. Here, $A_j$ (unitless) and $E_{A,j}$ (kJ·mol$^{-1}$) are the kinetic parameters and $T_R$ is used in Kelvin.

$$k_j = \exp\left(A_j - \frac{E_{A,j}}{R}\left(\frac{1}{T_R} - \frac{1}{T_{ref}}\right)\right) \; [h^{-1}] \tag{5}$$

Since all chemical reactions are assumed to occur exclusively in the liquid phase, which contains the overwhelming majority of the system mass and is dominated by water, the gas phase acts solely as a non-reactive pressure boundary. The gas phase consists only of water vapor and small amounts of non-condensable gases. Furthermore, its total amount of substance is negligible compared to that of the liquid phase. Consequently, gas-phase non-idealities do not influence reaction kinetics or mass balances, and the ideal gas law provides a sufficient description of the gas phase. The total pressure in the gas phase was therefore specified by the vapor pressure of water $p_{v,H_2O}$ which was calculated using the Antoine equation [77] (see Eq. (6)). Owing to the very high water content of the liquid phase, the activity of water remains close to unity, and the presence of non-volatile organic compounds has a negligible effect on the vapor pressure. Thus, the vapor pressure of pure water was used.

$$p_{v,H_2O} = 0,00133322 \bullet 10^{8,14019 - \frac{1810,94}{T_R - 28,665}} \; [bar] \tag{6}$$

The total amount of substance in the gas phase $n_{gas,tot}$ can be calculated using the ideal gas law (see Eq. (7)). The volume of the gas phase was calculated as follows with $V_G = V_R - V_L$, with reactor volume $V_R$ = 25$mL$ and $T_R$ is used in Kelvin:

$$n_{gas,tot} = \frac{V_G \bullet p_{vap}}{R \bullet T_R} \quad [mol] \tag{7}$$

The proportion of gaseous water in the total amount of substance is calculated from the difference between the total amount of gases and the individual gas components with the exception of water (see Eq. (8)).

$$n_{H_2O,gas} = n_{gas,tot} - \sum_{i=H_2,CH_4,CO_2} \frac{m_i}{M_i} \quad [mol] \tag{8}$$

The amount of water in the liquid phase is then:

$$m_{H_2O,liq} = m_{H_2O,total} - n_{H_2O,gas} \bullet M_{H_2O} \tag{9}$$

In the next step the component mass balances in the autoclave are applied to set the differential equations for each compound:

$$\frac{dm_i}{dt} = V_L \bullet \sum_j SC_{i,j} \bullet r_j \tag{10}$$

Here, $SC_{i,j}$ is a stoichiometric factor in mass units. A total of 13 differential equations (see Table 5) are used in the model. The equations were integrated with the built-in function *ode45* from Matlab, with absolute tolerance set to $10^{-6}$ and relative tolerance set to $10^{-3}$.

The kinetic parameters of each reaction $A_j$ and $E_{A,j}$ were estimated via minimization of the sum of squared errors. Eq. (11) shows the objective function $f(k)$ of which the minimum is determined numerically. $q$ is the number of experiments $l$ considered, $w_{i,l}$ is a specific weighting factor for each data point (see Table S5 in SI) and $m_{\mathrm{i,l,exp}}$ and. $m_{\mathrm{i,calc}}$ are the experimentally measured and calculated masses. Because the focus are the aromatics, the weights in the objective function are heavier for these compounds.

$$\min(f(k)) = \sum_{i=3}^{9} \sum_{l=1}^{q} w_{i,l} \left(\frac{m_{\mathrm{i,l,exp}} - m_{\mathrm{i,calc}}(k)}{m_{\mathrm{i,exp}}}\right)^2 \tag{11}$$

Not all components were considered in the optimization function. Lignin was fully converted, the intermediate oligomers could not be measured, nor could water (the concentration variation of which is also minimal). Furthermore, the focus of the model were the aromatics and not the gas products. Therefore, only components 3 to 9 were considered in the optimization function. The described model was implemented in MATLAB 2024A (version 24.1.0). The objective function was optimized

**Table 5**
Differential equation for each of the 13 reaction compounds which are part of the kinetic model.

| Compound number | Differential equation |
|---|---|
| 1 (Lignin) | $\frac{dm_1}{dt} = V_L * (-(r_1 + r_2 + r_3))$ |
| 2 (OL_int) | $\frac{dm_2}{dt} = V_L * (r_3 - (r_4 + r_5) - 0.13r_7 - 0.11r_8 - 0.1r_9)$ |
| 3 (3-Methoxycatechol) | $\frac{dm_3}{dt} = V_L * (r_4 - 0.89r_6)$ |
| 4 (Catechol) | $\frac{dm_4}{dt} = V_L * (r_5 + 0.71r_6 - (0.87r_7 + 0,6r_{10}))$ |
| 5 (Methylcatechol) | $\frac{dm_5}{dt} = V_L * (0.98r_7 - (0.89r_8 + 0,54r_{11} + r_{12}))$ |
| 6 (Dimethylcatechol) | $\frac{dm_6}{dt} = V_L * (0.99r_8 - (0.9r_9 + r_{13}))$ |
| 7 (Trimethylcatechol) | $\frac{dm_7}{dt} = V_L * (0.99r_9)$ |
| 8 (Solids) | $\frac{dm_8}{dt} = V_L * (r_2 + 0.83r_{12} + 0.83r_{13})$ |
| 9 (OL_fixed/misc. CH) | $\frac{dm_9}{dt} = V_L * (r_1)$ |
| 10 ($H_2O$) | $\frac{dm_{10}}{dt} = V_L * (0.14(r_{12} + r_{13} - (0.11r_6 + 0.4 * r_{10} + 0.47 * r_{11}))$ |
| 11 ($H_2$) | $\frac{dm_{11}}{dt} = V_L * (0.01(r_6 + r_8 + r_9 + r_{10}) + 0.02r_7 + 0.03(r_{11} + r_{12} + r_{13}))$ |
| 12 ($CH_4$) | $\frac{dm_{12}}{dt} = V_L * (0.26r_{10} + 0.21r_{11})$ |
| 13 ($CO_2$) | $\frac{dm_{12}}{dt} = V_L * (0.28r_6 + 0.73r_{10} + 0.76r_{11})$ |

using the non-linear least-squares solver *lsqnonlin*, which has proven to be fast and robust for the problem described. Table 6 shows the limits of the parameters $A_j$ and $E_{A,j}$. The threshold for experimental values was set to 0.1 wt% of the total biomass.

To optimize and to evaluate the robustness the model, a cross validation (CV) was applied, more precisely a 5-fold CV [78]. Cross-validation is commonly used in the field of kinetics [79,80]. In this case, 15 of the 17 experimentally determined points were randomly assigned to 5 different groups, each with 3 points. The optimization process was performed five times, each one omitting the points of one of the groups. To avoid large fluctuations for 3-methoxycatechol, Point 1 ($T_R = 300$ °C, $t_R = 0$ min) and point 6 ($T_R = 325$ °C, $t_R = 0$ min) were always included in the training database. For each kinetic parameter $\theta_j \in \{A_j, E_{A,j}\}$, the sample standard deviation across all five validation groups was computed:

$$s_j = \sqrt{\frac{1}{k-1}\sum_{i=1}^{k}(\theta_{j,i} - \overline{\theta_j})^2} \tag{12}$$

$k = 5$ is the number of groups and $\overline{\theta_j}$ is the mean parameter value. The confidence interval (CI) for each parameter $\theta_{j,i}$ was calculated based on the standard deviation of the estimates obtained from the five cross-validation groups, assuming a Student's t-distribution with four degrees of freedom. The general form of the two-sided confidence interval is given by Eq. (13) where $\alpha$ is the significance level, which is set to 0.05 in this study. $t_{\alpha/2,k-1}$ is the critical value from Student's t-distribution with $k-1$ degrees of freedom.

$$CI_{(1-\alpha)}(\theta_j) = s_j * \frac{t_{\alpha/2,\ k-1}}{\sqrt{k}} \tag{13}$$

The best performing parameter set, the one with the lowest objective function value $\min(f(k))$ was selected. If the absolute parameter value was smaller than the calculated CI, it was considered as statistically insignificant and it was removed from the model. This procedure was repeated iteratively, each time reoptimizing the reduced model, until all remaining parameters were statistically relevant.

**Table 6**
Boundaries for $A_j$ and $E_{A,j}$ and threshold for experimental data used for the optimization.

| | Lower bound | Upper bound |
|---|---|---|
| $A_j$ | -20 | 10 |
| $E_{A,j}$ | 0 kJ/mol | 1000 kJ/mol |

Three different statistical error calculations were carried out to evaluate the validity of the model. In addition to the R2 value, the mean absolute error (MAE) and the root mean square error (RMSE) were also calculated (Eqs. (14), (15), (16)) with n as the sample size.

$$R^2 = 1 - \frac{\sum (Y_{i,\exp} - Y_{i,calc})^2}{\sum (Y_{i,\exp} - \overline{Y_{i,\exp}})^2} \tag{14}$$

$$MAE = \frac{1}{n}\sum_{i=1}^{n} \left| Y_{i,\exp} - Y_{i,calc} \right| \tag{15}$$

$$RMSE = \sqrt{\frac{1}{n}\sum_{i=1}^{n} (Y_{i,\exp} - Y_{i,calc})^2} \tag{16}$$

## 3. Results & discussion

### 3.1. Carbon mass balance

The carbon mass balances of the various HTL experiments (see Fig. 7) confirm the observations and conclusions drawn in the previous study [65]. The influence of temperature $T_R$ clearly outweighs the influence of the holding time $t_R$, as can be seen, for example, from the decrease in the organic carbon content in the liquid phase from 30 to over 40 wt% at $T_R = 300$ °C and $T_R = 325$ °C to below 20 wt% at $T_R = 350$ °C. Even if the reaction is stopped directly after the heating time, the value at $T_R = 350$ °C for the organic carbon is just under 30 wt%. The carbon content in the solid is also higher at the highest temperature in almost all cases than at the others, regardless of the holding time $t_R$, which indicates an increased repolymerization rate. The decisive factor here is the high density of functional groups on the oligomers and monomers [58]. At the same time, aromatics are likewise a source of char and tar formation, especially at higher temperatures [81]. In addition, typical pyrolysis reactions, such as radical-induced reactions, further contribute to increased char formation [82]. This may be one reason why more carbon ends up in the solid, especially at higher temperatures. The experiments at $T_R = 300$ °C and holding times from $t_R = 10$ min are an exception

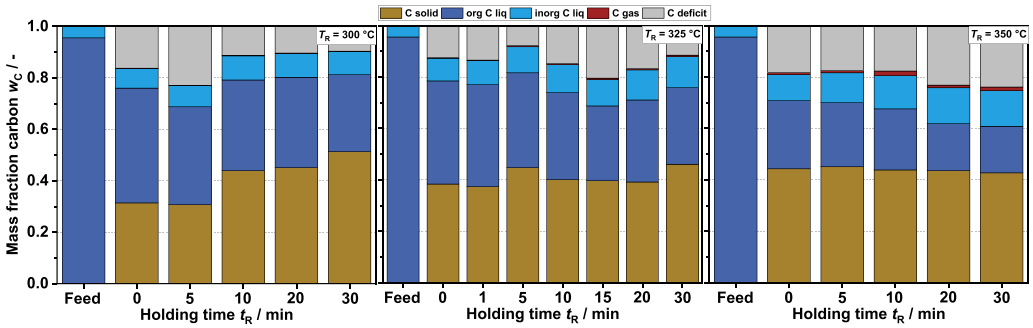


**Fig. 7.** Carbon mass fractions at different reaction temperatures $T_R$ and different holding times $t_R$ and before processing (feed); brown: C mass fraction solid; green: organic C mass fraction liquid phase; blue: inorganic C mass fraction liquid phase; red: C mass fraction gas phase (calculated from the detected gas compounds); and gray: deficit of carbon.

here. While the carbon content in the solid is largely constant at the other reaction temperatures investigated, a clear increase can be seen here. The lower reaction rate of repolymerization could be one reason for this observation. The gases hardly play a role with regard to the distribution of carbon. This applies both to permanent gases, where only $CO_2$ and no CO was detected, and to hydrocarbons. Among the latter, $CH_4$ is the most frequently produced gas. For this reason, too, it was decided to focus the model mainly on the aromatics and to allow the gases to occur only as by-products.

### 3.2. Experimental yields aromatic compounds GC-FID

The most interesting part of the carbon mass balance for this study is the dark blue section, which represents the organic carbon. Approx. 5 – 30 wt% of the carbon in this section can be traced back to aromatic monomers. GC-FID and GC-MS were used to identify and quantify these compounds. Based on the previous work, we know that the primary monomers are catechols. While we mainly focused on the influence of temperature, in this study we also looked at the influence of holding time. Fig. 8 shows the yields of various aromatic monomers at $T_R = 300$ °C, 325 °C and 350 °Cand holding times of $t_R = 0 – 30$ min. The highest yield of a single substance, in this case 22.0 mg catechol per g biomass, was achieved at $T_R = 325$ °C and a holding time of $t_R = 1$ min. In principle, it can be stated that the yields are highest at $T_R = 325$ °C compared to the other two investigated temperatures. While at $T_R = 300$ °C intermediates with methoxy groups such as syringol or 3-methoxycatechol are still present, at $T_R = 350$ °C repolymerization or decomposition, e.g. by hydrolysis, is more pronounced. The second point can be confirmed by the fact that the methylated catechols in particular have not yet passed through a maximum at the two lower temperatures at $t_R = 30$ min or that largely stable yields can be observed over several of the holding times investigated. Overall, the results fit well with the reaction scheme in Fig. 4. The intermediates such as 3-methoxycatechol are clearly visible and, in contrast to the other catechols, they decrease rapidly even at a low reaction temperature of $T_R = 300$ °C. This indicates the instability of the methoxy group under the given conditions. As in the postulated reaction mechanisms in Fig. 5, this can occur either by hydrolysis or by the formation of radicals, which then contribute to the formation of the methyl catechols further down the line. The low yields of syringol and guaiacol with 2 mg per g biomass or less and only detectable at $T_R = 300$ °C support the decision of not considering these two substances in their own right in this model. A more detailed discussion about the monomer yields compared to state-of-the-art research on this topic can be found in our previous study [65].

### 3.3. Evaluation of the kinetic modelling

Fig. 9, Fig. 10 and Fig. 11 show the yield curves of the individual components based on the developed kinetic model. In addition, the measured yields including error bars are also shown. Four graphs are shown for each of the three reaction temperatures. All components involved in the reaction components are plotted with the exception of water. Table 7 lists the calculated errors ($R^2$, MAE and RMSE) for the aromatic monomers. Due to the assumption that the original kraft lignin is no longer present in the black liquor after heating starts, its degradation is very rapid over all three temperatures and does not show any major differences. Consequently, there are also hardly any visible differences for the solid and the fixed oligomers and other hydrocarbons, as

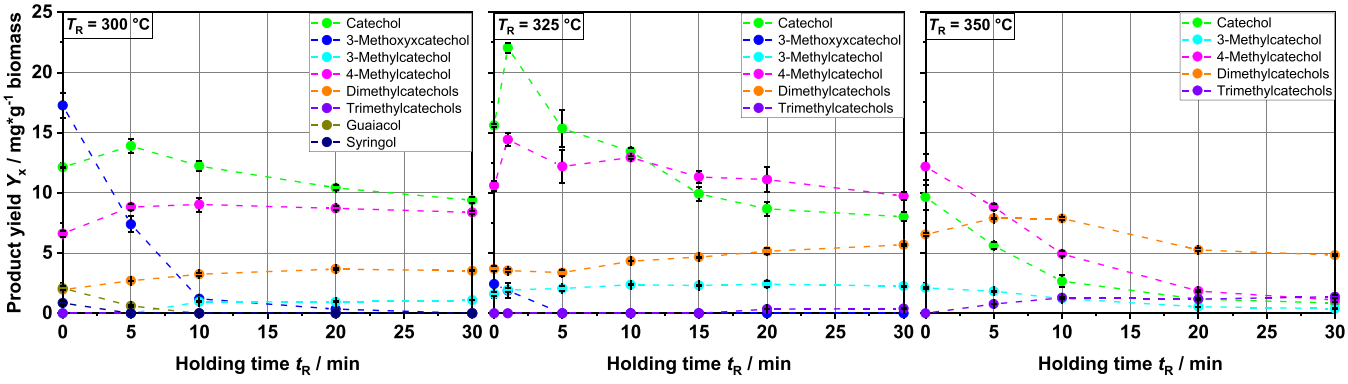


**Fig. 8.** Product yields in mg per g biomass of the different aromatic monomers with focus on compounds with methoxy groups and hydroxy groups. The experimental results at different holding times $t_R$ at three different reaction temperatures $T_R = 300$ °C, 325 °C and 350 °C (from left to right) are shown. The analysis was done by GC-FID.

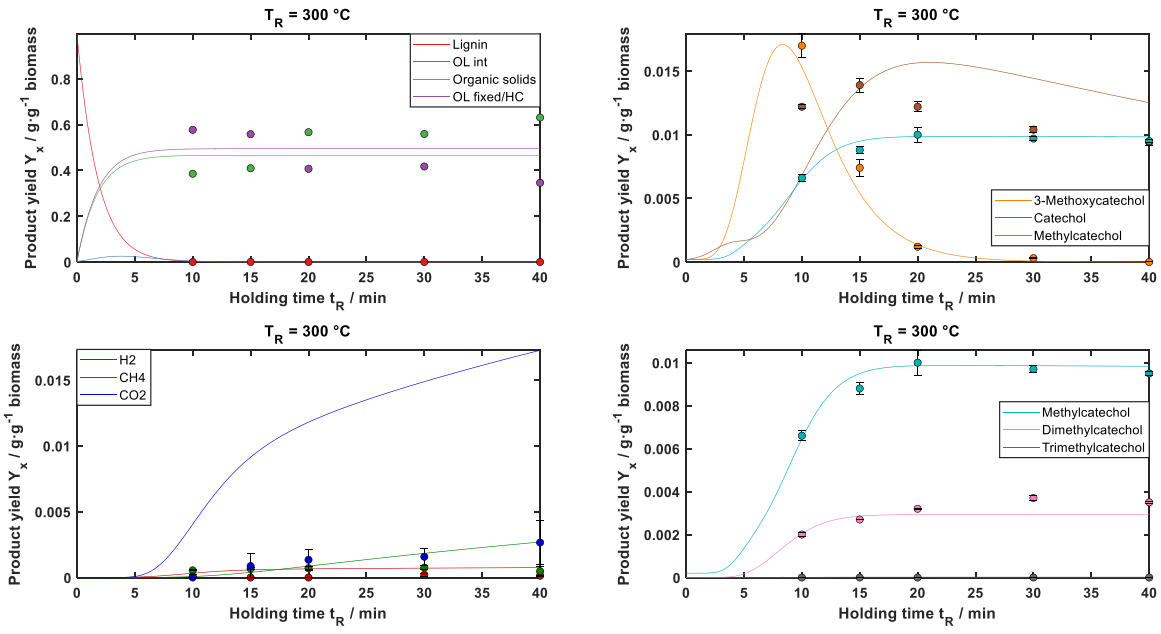


**Fig. 9.** Comparison between calculated kinetic model fits (lines) and the experimental results (dots) for the batch experiments at reaction temperature $T_R = 300$ °C and holding times $t_R = 0 - 30$ min. No experimental values for OL_int. The heating phase from 0 to 10 min is included; top left: oligomeric structures; top right: main aromatic monomers; bottom left: gaseous compounds; bottom right: methylated catechols.

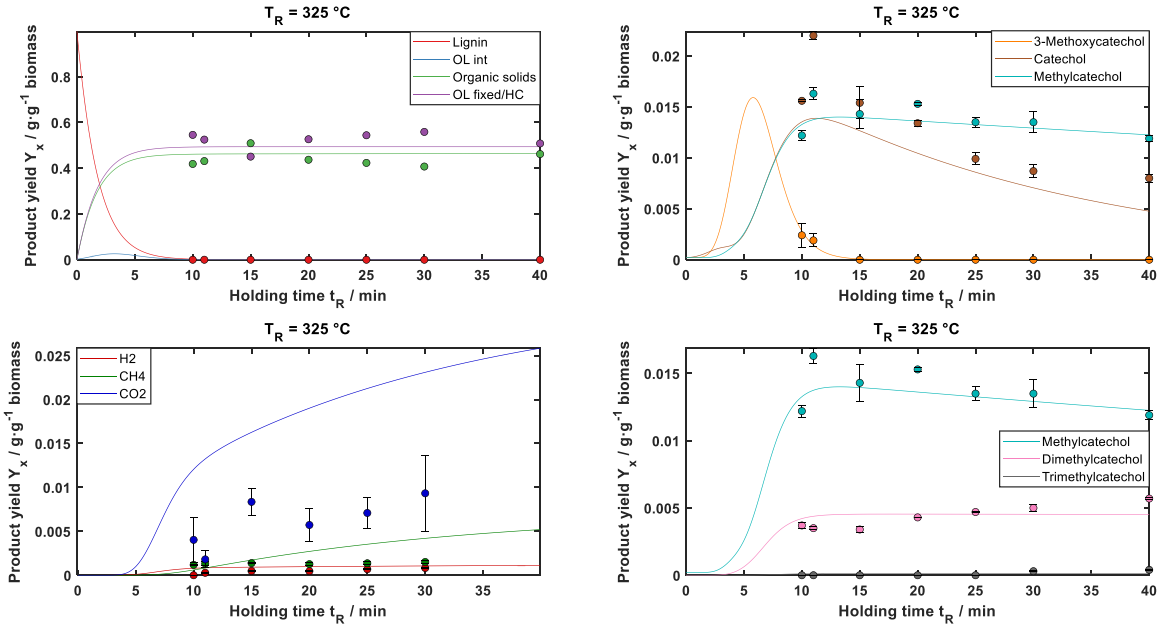


**Fig. 10.** Comparison between calculated kinetic model fits (lines) and the experimental results (dots) for the batch experiments at reaction temperature $T_R = 325$ °C and holding times $t_R = 0 - 30$ min. No experimental values for OL_int. The heating phase from 0 to 10 min is included; top left: oligomeric structures; top right: main aromatic monomers; bottom left: gaseous compounds; bottom right: methylated catechols.

these are formed primarily from the lignin. The intermediate OL_int is visible at all three temperatures, although the reaction times are slightly shorter with increasing $T_R$, as can be seen from the slightly faster decrease in yield. The very stable values for fixed oligomers and solids after the heating time fit well with the carbon mass balances. Only at $T_R = 300$ °C is the increase in the solid phase in the carbon mass balance not visible in the calculated data from the kinetic model for solids and fixed oligomers.

The main focus of the work is on the aromatic monomers. Together with the results of the simulation for the gaseous compounds, a good overview of the depolymerization of lignin under hydrothermal conditions is obtained. The gas components $H_2$, $CH_4$, and $CO_2$ are clearly overdetermined at $T_R = 300$ °C and 325 °C, but at $T_R = 350$ °C the simulated values for $H_2$ and $CO_2$ correlate well with the experimental results. The significantly higher yields of the two components at lower temperatures can be explained by methanol reforming in supercritical water, which is accelerated at higher temperatures [75]. Methanol reforming is already integrated in the model directly from $T_R = 300$ °C, as the model did not take account of methanol as a theoretical product of 3-methoxycatechol to catechol, due to the points already mentioned. The values for methane are clearly too high. This is a product of the gasification reactions of catechol and methylcatechol. Studies on the

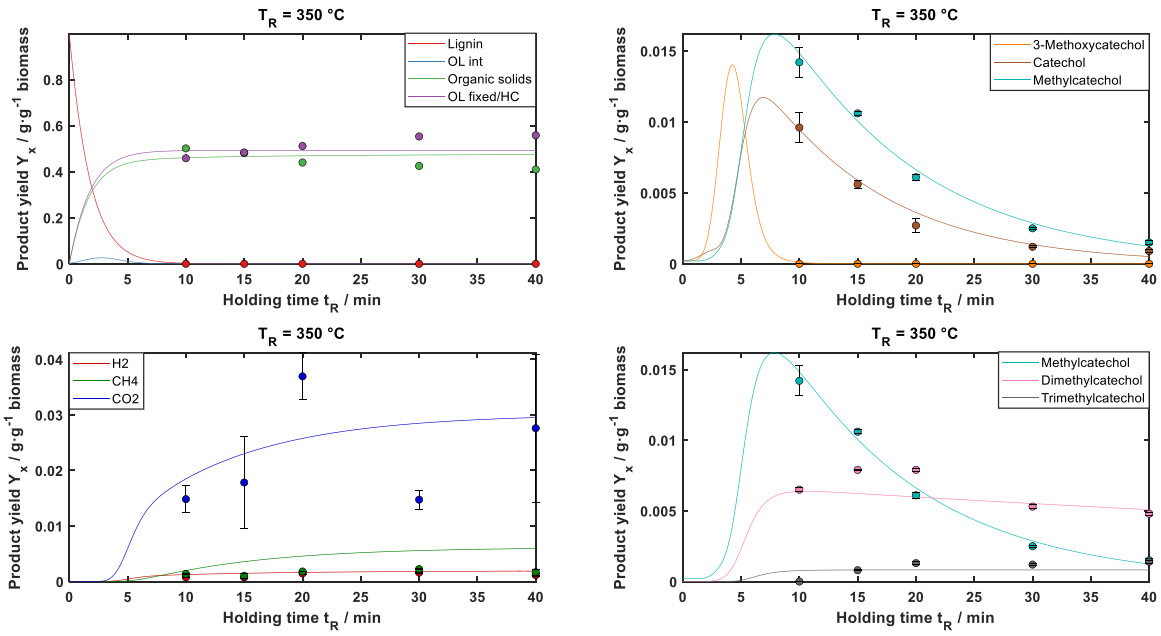


**Fig. 11.** Comparison between calculated kinetic model fits (lines) and the experimental results (dots) for the batch experiments at reaction temperature $T_R = 350$ °C and holding times $t_R = 0 – 30$ min. No experimental values for OL_int. The heating phase from 0 to 10 min is included; top left: oligomeric structures; top right: main aromatic monomers; bottom left: gaseous compounds; bottom right: methylated catechols.

**Table 7**
Error estimations for the simulated aromatic monomer compounds at different reaction temperatures $T_R$.

| | 300 °C | | | 325 °C | | | 350 °C | | |
|---|---|---|---|---|---|---|---|---|---|
| | $R^2$ | *MAE / g*g$^{-1}$* | *RMSE/ g*g$^{-1}$* | $R^2$ | *MAE/ g*g$^{-1}$* | *RMSE/ g*g$^{-1}$* | $R^2$ | *MAE/ g*g$^{-1}$* | *RMSE/ g*g$^{-1}$* |
| **3-Methoxycatechol** | 0.97 | 0.0008 | 0.0011 | 0.94 | 0.0001 | 0.0002 | n.a. | n.a. | n.a. |
| **Catechol** | -4.5 | 0.0033 | 0.0037 | 0.30 | 0.0032 | 0.0038 | 0.98 | 0.0004 | 0.0005 |
| **Methylcatechol** | 0.92 | 0.0003 | 0.0003 | 0.28 | 0.001 | 0.0012 | 0.99 | 0.0005 | 0.0005 |
| **Dimethylcatechol** | 0.4 | 0.0004 | 0.0005 | 0.09 | 0.0007 | 0.0008 | 0.24 | 0.0008 | 0.0011 |
| **Trimethylcatechol** | n.a. | n.a. | n.a. | 0.02 | 0.0001 | 0.0002 | 0.02 | 0.0004 | 0.0005 |

gasification of catechol under hydrothermal conditions by Kruse et al. at 700 °C and 400 bar have shown that virtually no methane is produced at very low catechol concentrations [83]. This may also apply to milder conditions, such as those used for hydrothermal liquefaction. However, since we assume a methane source and given that the combination of methyl and hydrogen radicals to methane cannot be represented due to a lack of data, methane is present as a product of the gasification of the monomers. In addition, due account needs to be taken of the fact that it is difficult to detect and quantify all of these gases due to the very small quantities of gas formed. The main focus is on the monomers, for which, in contrast to the other components, there are meaningful error calculations (see Table 7). To emphasize the methylation reactions, the three methylcatechols are shown in a fourth image (bottom right) in the figures.

At all three different temperatures, it is evident that many decisive reactions already take place during the heating time. This is particularly clear with 3-methoxycatechol, which shows a significant maximum within 10 min at all three reaction temperatures. The decisive factor here are the high experimental values at $T_R = 300$ °C. Due to the high syringyl group content in the black liquor used, this is the logical consequence, as the methoxy groups are already split off at lower temperatures or are converted to hydroxyl groups. In a study on pyrolysis reactions by Pan et al. with catalysts, the decomposition of syringol to phenolic compounds was investigated at higher temperatures (above 300 °C) with the result that radical reactions typical of pyrolysis in particular take place [74]. In addition, other studies on demethoxylation with different catalysts already show syringol decomposition at below 300 °C [84–86]. Due to the special properties of water, we assume that in our case both are possible at temperatures below or around 300 °C and for this reason the intermediates guaiacol and syringol are already almost completely degraded after the heating phase and 3-methoxycatechol as a prominent intermediate of syringol degradation also reaches its maximum. The coefficient of determination for 3-methoxycatechol is $R^2 > 0.9$ for $T_R = 300$ °C and $T_R = 325$ °C. In contrast, the developed model overestimated and underestimated catechol at these two temperatures. Nevertheless, the model is satisfactory as the curves match the experimental values. Although the $R^2$ value for $T_R = 325$ °C is 0.3 and even negative at $T_R = 300$ °C, the absolute (MAE) and weighted error (RMSE) is not too high between 0.032 and 0.038 g/g biomass. One major issue with the $R^2$ value is the high fluctuation for extremely low values for example di and trimethylcatechol yields. Since $R^2$ actually represents the deviations of the model compared to the deviations that a simple average value would yield, when the experimental values are always near each other and have low values, it follows that small deviations can lead to very bad $R^2$ values, The same thing occurs when the curve estimated by the model has the right shape but does not pass through the data points like the catechol at $T_R = 300$ °C and 325 °C. Therefore, we decided to use MAE and RMSE values as well, which are measurements of absolute error. These show that our model is not too far removed from the experimental data.

Kinetic modeling shows that the additional route via OL_int to catechol is probably not sufficient to reach the peaks of the experimental values at $t_R = 0 – 5$ min. Due to the fact that the experiments only produced very low values for guaiacol (see Fig. 8), it would be conceivable to improve the model by conducting experiments at lower temperatures, such as in the previous study where temperatures go

down to $T_R = 250$ °C [65]. Based on this type of data, the reaction pathway assumed by Schuler et al. could possibly be represented [87, 88]. On the other hand, however, it must be considered that the near-critical range is already further away at a reaction temperature of $T_R = 250$ °C and ionic reactions probably dominate. This raises the question of whether it makes sense to lower the temperature range to this extent for a model to describe the depolymerization of lignin under near-critical conditions. A more appropriate approach than lowering the temperature would be to investigate the yields occurring during the heating phase. However, these experiments need to be designed for the phase transition and the near-critical range in order to avoid fluctuations caused by these transitions as far as possible. At $T_R = 350$ °C, when the radical-induced reactions in particular are dominant, for instance the methylation of the catechol, the model provides a very good result with an $R^2 = 0.98$ and very low errors. The same also applies to the various methylcatechols as secondary products. This shows clearly that the strength of the model lies in these primarily radical reaction steps. The single methylated catechols in particular are very accurately represented by the kinetic model ($R^2 = 0.28 – 0.99$, MAE, RMSE $\leq 0.0012$ g/g biomass). The calculated values for the di- and trimethylcatechols are also within the range of the experimental values. Although the $R^2$ values are extremely low in some cases, due account must be taken here of the fact that fluctuations at these low yields, especially for trimethylcatechol, have a large influence on the R2 value. In contrast, the MAE and RMSE values are significantly better. An important point that still needs to be discussed here is the repolymerization of the multiple methylated catechols. In the initial model, repolymerization of dimethylcatechols is present, but not for trimethylcatechols. This decision was based on the temperature range studied up to $T_R = 350$ °C. We know from other experiments that the yields of all aromatic monomers decrease sharply at higher temperatures [65], but this step is not relevant for the model in the temperature interval studied, as the cross validation will also show later.

The parity plots in Fig. 12 confirm the impression that the model accounts very well for methylation in particular. Furthermore, it seems to be a reasonable approach to combine 3-methylcatechol and 4-methylcatechol into one group. The results are satisfactory and at the same time this makes the model less complex. In addition to the successful integration of the methylation, the second new finding, the kinetic model also represents the degradation of syringyl groups to catechol via 3-methoxycatechol very effectively. The major deficiency is catechol at $T_R = 300$ °C and 325 °C, which is illustrated clearly by the parity plots. The scattering over -20 % and + 20 % deviation from the experimental values is clearly evident. The model can still be optimized in this area. Overall, it can be stated that the model satisfactorily represents the various aromatic monomers that are formed during the

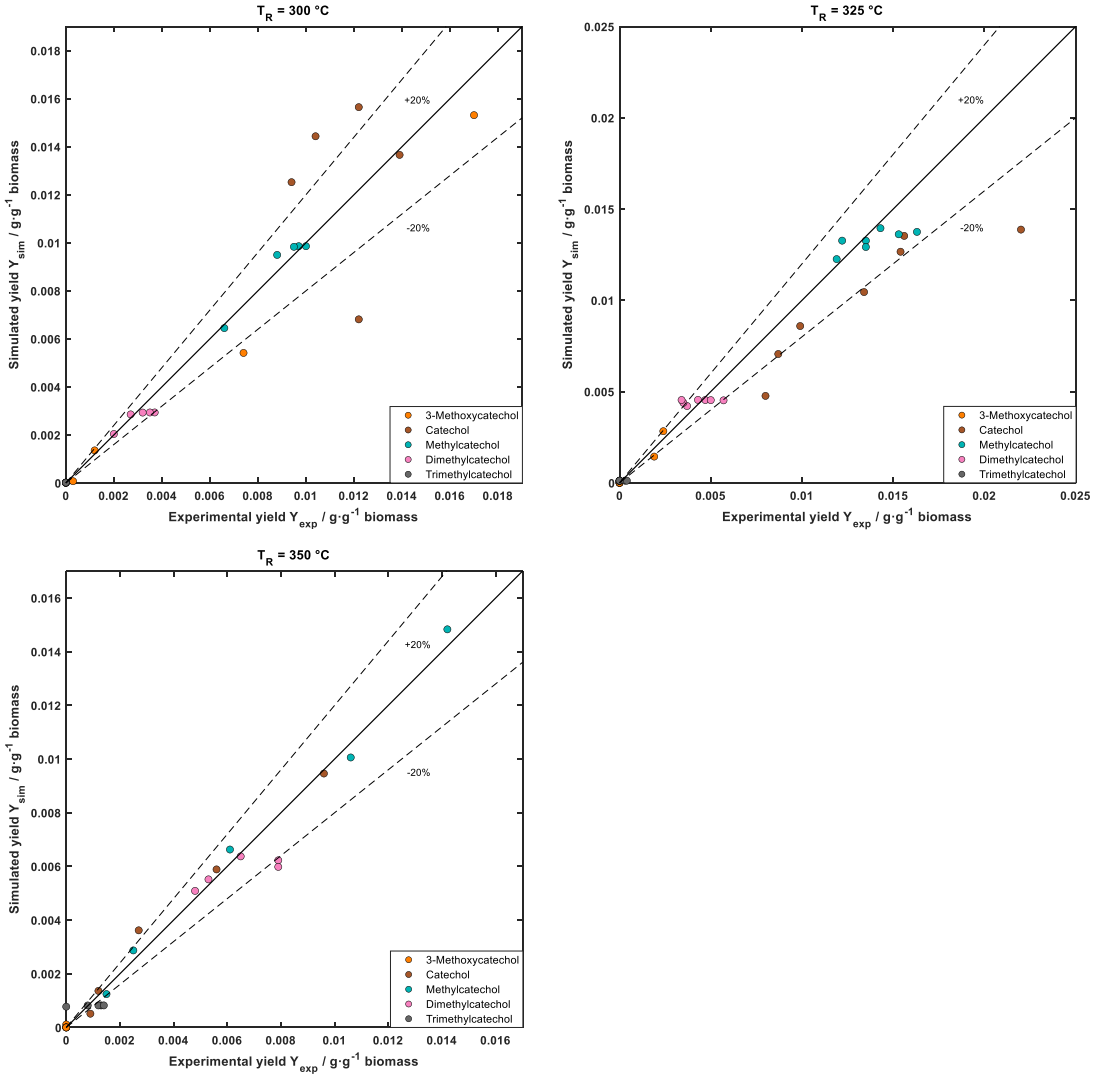


**Fig. 12.** Simulation vs experimental results at reaction temperature $T_R = 300$ °C, 325 °C and 350 °C.

depolymerization of lignin in BL under the given conditions in batch experiments. Due to the similar product distribution in initial continuous experiments (see Wörner et al. [65]), the model is well suited for making initial predictions as to how a continuous experimental plant tailored to specific products should be designed.

### 3.4. Results of 5-fold cross validation

The 5-fold CV can be used to identify statistically irrelevant parameters and reaction paths in line with the kinetic parameters and the model can be optimized if necessary. Fig. 13 shows the optimized reaction scheme. The gray dashed lines and reactions show those that were removed from the model using the CV. For a deeper analysis of the model, an interpretation of the calculated kinetic parameters and the rate constants for each of the three reaction temperatures is provided (see Table 8). The kinetic parameters for all 13 reactions in the original reaction network before applying CV can be found in the Supporting Information in Table S7. Additionally, the positive or negative change in the estimated errors compared to the errors from the non-validated model can be found in Table S8 Looking at the parameter table (see Table 8), it can be seen that the reaction constants for the first two reactions are 0 kJ/mol and therefore have no influence on the model, regardless of the temperature. The same applies to R5 with an $E_{A,5}$ = 0.01 kJ/mol. In this case, even the entire reaction pathway from OL_int to catechol is not statistically relevant, as the model is almost exclusively about 3-methoxycatechol. Accordingly, this can be removed completely. Interestingly, the catechol peak at $t_R = 1$ min and $T_R = 325$ °C cannot be achieved with this reaction pathway, something which was originally deemed to be feasible. Instead, this pathway has little to no effect on the model. In contrast to R5, the other two removed reaction steps R11 and R13 have exceedingly high activation energies. However, both reactions play scarcely no role in the investigated temperature range. Possibly both would become more relevant at a higher reaction temperature. However, since the yield of aromatic compounds decreases drastically with increasing reaction temperature, both reactions can be removed to optimize the model. In the case of R11, it is likely that the gas production via catechol decomposition in R10 is already sufficient and therefore the decomposition of methylcatechol is neglected in the model. Overall, the performance of the model has become even better and faster without having too great an impact on the results. These results can be found in the Figure S3-1–3 and Table S6 in SI.

The depolymerization of the lignin (R3), as well as the direct conversion to the fractions of fixed oligomers and solids (R1 & R2), which do not contribute further to the formation of aromatic monomers, exhibit extremely low activation energies $E_{A,j}$. This suggests that under the given conditions the activation energy for depolymerization has scarcely no role to play and proceeds independently of it. In accordance with the model, it is also the case that a large proportion of biomass is removed from the reaction network directly at the beginning, presumably already in the heating phase, remaining in the solid or the fixed oligomers. Noticeable are the high-rate constants of the reactions over 3-methoxycatechol to methylcatechol (R4, R6, R7) with $k_j > 1$ min$^{-1}$, especially at $T_R = 350$ °C. In the case of R4 and R6, this can be explained by the veryhigh peak of 3-methoxycatechol and the subsequent rapid

**Table 8**
Activation energies $E_{A,j}$, Arrhenius factor $A_j$ and the respective rate coefficients $k_j$ for each reaction temperature for the 10 reactions of the developed model after cross validation.

| Reaction Number | $E_{A,j}$ / kJ*mol$^{-1}$ | $A_j$ / - | k (300 °C) / min$^{-1}$ | k (325 °C) / min$^{-1}$ | k (350 °C) / min$^{-1}$ |
|---|---|---|---|---|---|
| 1 | 0 | 4.38 ± 0.13 | $1.33 \bullet 10^{0}$ | $1.33 \bullet 10^{0}$ | $1.33 \bullet 10^{0}$ |
| 2 | 0 | 4.30 ± 0.15 | $1.23 \bullet 10^{0}$ | $1.23 \bullet 10^{0}$ | $1.23 \bullet 10^{0}$ |
| 3 | 15.54 ± 2.81 | 4.02 ± 0.41 | $8.10 \bullet 10^{-1}$ | $9.28 \bullet 10^{-1}$ | $1,05 \bullet 10^{0}$ |
| 4 | 33.12 ± 8.96 | 3.42 ± 0.22 | $3.81 \bullet 10^{-1}$ | $5.10 \bullet 10^{-1}$ | $6.66 \bullet 10^{-1}$ |
| 6 | 125.29 ± 10.38 | 4.11 ± 0.03 | $3.38 \bullet 10^{-1}$ | $1.01 \bullet 10^{0}$ | $2.79 \bullet 10^{0}$ |
| 7 | 14.85 ± 17.35 | 3.84 ± 0.41 | $6.78 \bullet 10^{-1}$ | $7.72 \bullet 10^{-1}$ | $8.71 \bullet 10^{-1}$ |
| 8 | 13.65 ± 16.67 | 2.44 ± 0.31 | $1.70 \bullet 10^{-1}$ | $1.91 \bullet 10^{-1}$ | $2.14 \bullet 10^{-1}$ |
| 9 | 234.95 ± 42.09 | 0.69 ± 0.54 | $4.21 \bullet 10^{-3}$ | $3.34 \bullet 10^{-2}$ | $2.24 \bullet 10^{-1}$ |
| 10 | 121.46 ± 13.82 | 1.30 ± 0.06 | $2.11 \bullet 10^{-2}$ | $6.12 \bullet 10^{-2}$ | $1.63 \bullet 10^{-1}$ |
| 12 | 344.60 ± 45.69 | -1.17 ± 0.34 | $2.51 \bullet 10^{-4}$ | $5.15 \bullet 10^{-3}$ | $8.30 \bullet 10^{-2}$ |

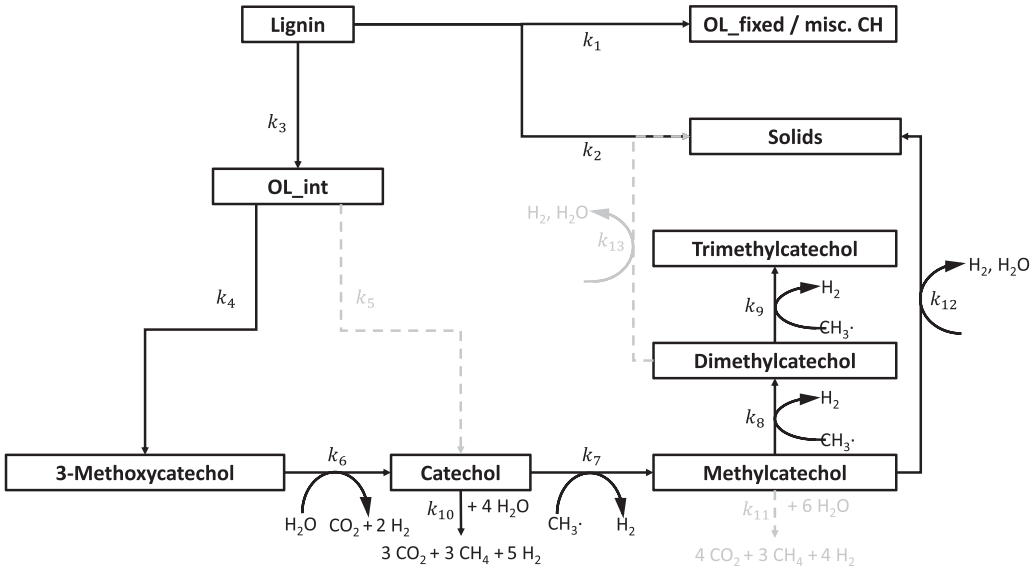


**Fig. 13.** Updated reaction scheme after 5-fold cross validation. The light gray reaction paths were classified by CV as not relevant for the kinetic model.

decrease over a few minutes. Accordingly, the experimentally recorded values also cause the reaction constants to increase. For R7, catechol to methylcatechol, on the other hand, the already high yield of methylcatechol shortly after the heating phase probably plays a role. There may also be another reaction pathway to methylcatechol that was not revealed by the experiments conducted. Interestingly, the assumed effect due to repolymerization via the aromatic compounds is very low (R12 & R13). This is shown by the high activation energies together with the low-rate constants up to the order of $10^{-6}$ $min^{-1}$. The kinetic model here definitely favors the formation of solids via the direct path from the lignin. However, this evaluation needs to take account of the small proportion of the total mass accounted for by the compounds on which the work is focusing. Repolymerization will almost certainly have a major influence, especially with regard to higher temperatures. Repolymerization is also conceivable within reactions R1 and R2. The same applies to the decomposition of methylcatechols into gases (R11, see Table S7 in SI). In contrast, the decomposition of catechol into gases is more relevant (R10).

### 3.5. Comparison with other kinetic studies of lignin depolymerization

For validation of the model, studies on the depolymerization of lignin under hydrothermal conditions, which have also developed a kinetic model, are used. In their two studies, Wahyudiono et al. investigated the kinetic parameters of the conversion of model substances under hydrothermal conditions. The study on catechol [71] was carried out at higher temperatures between $T_R = 370 – 420$ °C at a pressure of 300 bar. The rate constant $k$ for the catechol conversion is in the order of $10^{-4}$ – $10^{-3}$ $min^{-1}$. This is significantly smaller compared to the calculated values of this work for reaction R7 and R10. The activation energy of 50.72 kJ/mol, on the other hand, is much closer to this study, comparable to $E_{A,7}$ of 56.24 kJ/mol. The comparison with the parameters for the conversion of guaiacol in the second study [72] reaches a similar conclusion, despite the fact that temperatures in the subcritical range are also investigated here ($T_R = 210 – 400$ °C). However, in this case as well, the kinetic parameters do only approach those from this study for the reactions R4 – R6, which are closest to a conversion of methoxyphenols, at high temperatures in the supercritical range. A major difference here is that a pressure of 8 MPa was used in the low temperature range. Furthermore, this process does not include salts or other catalytically active substances that can accelerate or favor the reactions to certain products. Yong and Matsumura have determined higher rate constants in their work on the depolymerization of lignin under subcritical and supercritical conditions in water [68]. The values for lignin decomposition to guaiacol are between 6.42 $min^{-1}$ ($T_R = 300$ °C) and 12.18 $min^{-1}$ ($T_R = 370$ °C). Comparable to this are R3 and R4, which describe the lignin decomposition to 3-methoxycatechol. In particular, R4 with a rate constant of $k = 1.09$ $min^{-1}$ at $T_R = 350$ °C is close to the values from the study. In their work, they also included the lumped group TOC in their reaction network, which describes the other organic products in the liquid phase. The comparison with R1 is therefore useful, as the other organic products based on the biomass are also included here. The rate constants of $6.35 \cdot 10^{-1}$ $min^{-1}$ to 1.09 $min^{-1}$ (300 – 370 °C) enclose the rate constant calculated for our case, which is independent of the activation energy. However, due to the special design of their experimental apparatus for these kinetic measurements, exceedingly small continuous flow reactor with 0.5 – 10 s residence time, mass and heat transfer effects can occur to different degrees compared to the batch operation used in this study. A study comparable to this one in terms of experimental design is that of Forchheim et al. [56]. In this study, a formal kinetic model with pseudo-first order was also developed on the basis of batch experiments on lignin depolymerization under hydrothermal conditions. However, the resulting rate constants are lower than in this study, e.g. the reaction of lignin to methoxyphenols to catechol. A consistent finding is the negligible repolymerization from the monomers to solids in accordance with the models compared to the reaction from lignin directly or via oligomers to solids. Interestingly, the calculated and experimental yields for catechol remain largely constant in their work, which is definitely not valid in the case of this study. The reasons for the larger differences despite the similar setup could be related to the feedstock, which is enzymatically produced lignin and not kraft lignin. The literature hardly contains any work that deals with the methylation of catechol in kinetic models for lignin depolymerization. The conversion of a hydroxyl group to a methyl group and the resulting cresols are discussed more frequently. This is also imaginable for a hypothetical pathway from syringol to pyrogallol (benzene ring with three hydroxy groups) and a subsequent conversion to methylcatechols, but would not be applicable to the results described here. As already mentioned, the multiple methylated catechols strongly indicate radical reactions. One work in which at least the reaction of catechol to methylcatechol is integrated in a kinetic model is that of Schuler [89]. For $T_R = 300$ °C the reaction constant is $k = 3.54 \cdot 10^{-3}$ $min^{-1}$, and at $T_R = 350$ °C $k = 2.63 \cdot 10^{-2}$ $min^{-1}$. Thus, the values are clearly below those from the model developed here for R6. Even the rate constants for R7 and R8 are significantly higher. The heating period, which is not in a sand bath but in a GC oven, i.e., heat transfer via air, may have played a role in the differences. Overall, it can be stated that the results provided by the developed kinetic model correlate well with the literature data. The difficulty in comparison is mainly due to the different experimental setups as well as the different lignin types. In terms of the results, this study tends to be more in line with the very fast, often continuously operated reactors with a low flow rate, such as those of Yong et al. or Abad-Fernandez et al. who also achieved similarly high or even higher values for lignin polymerization to monomers and used a reactor with an ultra-fast heating time [68,90,91].

### 3.6. Comparison with softwood data

In the last part of this paper, a comparison is made with data from tests with softwood. In the previous study, it was shown that the yields of aromatics obtained from the depolymerization of lignin when using black liquor directly differed only slightly when using BL based on softwood or hardwood [65]. The major difference between the two is that 3-methoxycatechol does not occur as an intermediate in softwood experiments, as it can only be formed via syringyl groups. Therefore, it is reasonable to assume that a kinetic model based on the use of hardwood BL also provides suitable values for softwood BL. Accordingly, the route via 3-methoxycatechol was removed from the model developed in this work. As before, the kinetic parameters were calculated based on the results of the experiments with hardwood BL. Fig. 14 shows the simulated yield curves for $T_R = 350$ °C and compares them with the experimentally determined yields for HTL experiments with softwood BL at $T_R = 350$ °C and three different holding times $t_R = 1$, 5 and 10 min. In fact, the points are well within the trend of the curves, despite the presence of some deviations. Overall, this is a promising result, showing as it does that the yields based on softwood depolymerization can also be represented with only minor changes to the existing kinetic model. Possible improvements could be the introduction of guaiacol as a single component, as this is by far the most important intermediate for catechol formation in the depolymerization of softwood lignin. However, further experiments with softwood BL need to be conducted for this purpose. Finally, it is shown again that the depolymerization is less influenced by the type of wood, but rather by the other components in the black liquor, whereby the various salts should be emphasized in particular.

## 4. Conclusion

The kinetic model developed in this study gives adequate simulations of the depolymerization of lignin under HTL conditions. A unique aspect here is the direct use of black liquor in which the lignin is dissolved. As a result, in addition to the effect of the catalytic effect of the water under the given conditions, the high concentration of salts such as sodium

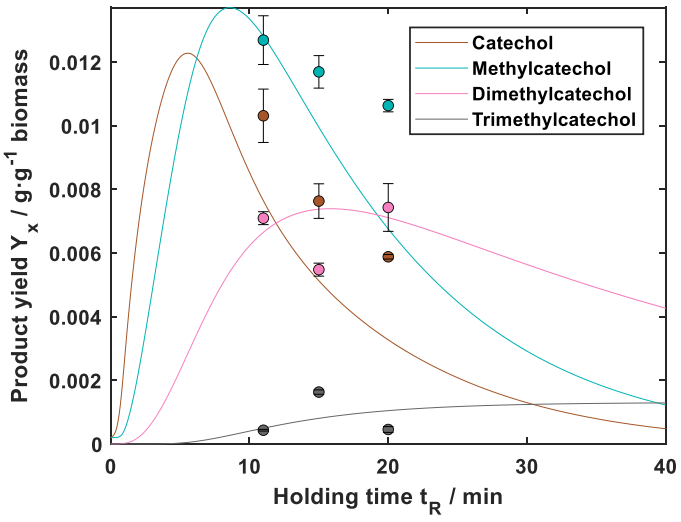


**Fig. 14.** Simulated yields based on the developed kinetic model without the 3-Methoxycatechol pathway (R4, R6) (lines) in comparison with experimental results of HTL with softwood BL. More information about these experiments can be found in Wörner et al. [65].

sulfide also influences depolymerization. The model describes the initial degradation of the lignin molecule to monomers, in the case of this work preferably catechols. The primary reaction pathway via 3-methoxycatechol, which has not yet been described in this way, was included in the model. In addition, the focus was on the subsequent methylation of catechol, probably due to radical reactions, as these are the main products among the aromatic monomers alongside catechol. Both experimental observations were successfully incorporated into the kinetic model. With the help of cross validation, it was afterwards possible to reduce the reaction scheme and the number of kinetic parameters, improving parameter identifiability without losing relevant information. The comparison with literature proved to be difficult, as although there are studies on lignin depolymerization in hydrothermal conditions, certain parameters are different. Nevertheless, similarities can be found in literature. The studies with very fast heating rates in particular show similar high-rate constants to those in this study, which are presumably due to the high salt concentration and the use of Kraft lignin. In addition, the literature also shows that the monomers and their formation only represent a small part of the entire reactions and products. The majority takes place in the oligomers and in the solid fraction. Although repolymerizations also take place between monomers, these contribute only slightly to the overall production of the solid. Finally, it was shown that the developed model may also provide useful results for the depolymerization of softwood lignin when black liquor is used directly in the HTL. For this purpose, only the path via 3-methoxycatechol had to be removed. This shows that it is primarily the salts in the black liquor that influence depolymerization. In summary, a promising kinetic model based on experimental data was developed in this work, which contains new proposed reaction pathways and whose range of application can possibly be extended.

## Abbreviations

| | |
|---|---|
| $T_R$ | Reaction temperature |
| $t_R$ | Holding time |
| $t_h$ | Heating time |
| GHG | Greenhouse gases |
| BTX | Benzene, Toluene, Xylene |
| MtA | Methanol to aromatics |
| HTL | Hydrothermal liquefaction |
| BL | Black liquor |
| GC | Gas chromatography |
| FID | Flame ionization detector |
| TCD | Temperature conductivity detector |
| ISTD | Internal standard |
| $Y$ | Product yield |
| MS | Mass spectroscopy |
| S | Syringyl- |
| G | Guaiacyl- |
| $w$ | Mass fraction |
| $R$ | Universal gas constant |
| $k$ | Reaction constant |
| $E_A$ | Activation energy |
| $A$ | Arrhenius factor |
| $r$ | Reaction rate |
| $m$ | Mass |
| $p$ | Pressure |
| $SC$ | Stoichiometric coefficient |
| $\rho$ | Mass concentration |
| $V$ | Volume |
| $n_i$ | Amount of substance |
| CV | Cross validation |
| CI | Confidence intervall |
| MAE | Mean absolute error |
| RMSE | Root mean squared error |
| $n$ | Sample size |

## CRediT authorship contribution statement

**Maximilian Wörner:** Writing – original draft, Visualization, Validation, Software, Methodology, Investigation, Formal analysis, Data curation, Conceptualization. **Bruno Lacerda de Oliveira Campos:** Writing – review & editing, Software, Methodology, Data curation, Conceptualization. **Ursel Hornung:** Writing – review & editing, Supervision, Resources, Project administration, Funding acquisition. **Nicolaus Dahmen:** Writing – review & editing, Supervision, Resources, Project administration, Funding acquisition.

## Funding

This research was funded by the European Union Horizon 2020 research and innovation program under grant agreement No. 884111, Black Liquor to Fuels (BL2F).

## Declaration of Competing Interest

The authors declare that they have no known competing financial interests or personal relationships that could have appeared to influence the work reported in this paper.

## Acknowledgements

We thank V. Holderied, B. Rolli, J. Heinrich and A. Lautenbach for their support during the sample analysis at IKFT, and T. Tietz and M. Pagel for their technical support.

## Appendix A. Supporting information

Supplementary data associated with this article can be found in the online version at doi:10.1016/j.jece.2026.122311.

## Data availability

Data will be made available on request.

## References


[1] K. Abbass, M.Z. Qasim, H. Song, M. Murshed, H. Mahmood, I. Younis, A review of the global climate change impacts, adaptation, and sustainable mitigation measures, Environ. Sci. Pollut. Res 29 (2022) 42539–42559, https://doi.org/10.1007/s11356-022-19718-6.

[2] M. Meinshausen, J. Lewis, C. McGlade, J. Gütschow, Z. Nicholls, R. Burdon, et al., Realization of Paris Agreement pledges may limit warming just below 2 °C, Nature 604 (2022) 304–309, https://doi.org/10.1038/s41586-022-04553-z.

[3] Alšauskas O. World Energy Outlook 2024 n.d.

[4] Energy Institute. Statistical Review of World Energy 2024 - 73th edition. 2024.

[5] H.-G. Franck, J.W. Stadelhofer, Industrial Aromatic Chemistry: Raw Materials · Processes · Products, Springer Berlin Heidelberg, Berlin, Heidelberg, 1988, https://doi.org/10.1007/978-3-642-73432-8.

[6] straits research, Benzene-Toluene-Xylene (BTX) Market Size, Share & Trends Forecasts (2022) 2021–2030. ⟨https://straitsresearch.com/report/benzene-toluene-xylene-market⟩.

[7] M. Bender, Global Aromatics Supply - Today and Tomorrow, Oil Gas. Eur. Mag. 39 (2013) 209–212.

[8] R.J. Schmidt, Industrial catalytic processes—phenol production, Appl. Catal. A Gen. 280 (2005) 89–103, https://doi.org/10.1016/j.apcata.2004.08.030.

[9] Phenol Market Size, Share, Analysis, Trend Forecast 2035 (2025). ⟨https://www.chemanalyst.com/industry-report/phenol-market-184⟩ (accessed November 9, 2025).

[10] H. Fiege, H.-W. Voges, T. Hamamoto, S. Umemura, T. Iwata, H. Miki, et al., Phenol Derivatives. Ullmann's encyclopedia of industrial chemistry, 7. edition, release 2015, Weinheim; Wiley Online Library: Wiley-VCH, 2010, https://doi.org/10.1002/14356007.a19_313.

[11] S. Wegelin, M.A.R. Meier, Bio-based aromatics for chemicals and materials: Advances in renewable drop-in and functional alternatives, Curr. Opin. Green. Sustain. Chem. 47 (2024) 100931, https://doi.org/10.1016/j.cogsc.2024.100931.

[12] S. Wang, G. Song, A pathway to bio-based aromatics, Nat. Sustain 6 (2023) 1295–1296, https://doi.org/10.1038/s41893-023-01191-9.

[13] Z. Li, Y. Jiang, Y. Li, H. Zhang, H. Li, S. Yang, Advances in Diels–Alder/aromatization of biomass furan derivatives towards renewable aromatic hydrocarbons, Catal. Sci. & Technol. 12 (2022) 1902–1921, https://doi.org/10.1039/D1CY02122B.

[14] T. Li, T. Shoinkhorova, J. Gascon, J. Ruiz-Martínez, Aromatics Production via Methanol-Mediated Transformation Routes, ACS Catal. 11 (2021) 7780–7819, https://doi.org/10.1021/acscatal.1c01422.

[15] T. Fu, Y. Guo, Z. Li, G. Zhan, Selective conversion of methanol to aromatics with superior catalytic stability by relay catalysis over quadruple ZSM-5 sequence beds with gradient-increasing acidity, Fuel 315 (2022) 123241, https://doi.org/10.1016/j.fuel.2022.123241.

[16] S. Heidenreich, P.U. Foscolo, New concepts in biomass gasification, Prog. Energy Combust. Sci. 46 (2015) 72–95, https://doi.org/10.1016/j.pecs.2014.06.002.

[17] V. Singh Sikarwar, M. Zhao, P. Clough, J. Yao, X. Zhong, M. Zaki Memon, et al., An overview of advances in biomass gasification, Energy & Environ. Sci. 9 (2016) 2939–2977, https://doi.org/10.1039/C6EE00935B.

[18] B. Lacerda de Oliveira Campos, K. John, P. Beeskow, K. Herrera Delgado, S. Pitter, N. Dahmen, et al., A Detailed Process and Techno-Economic Analysis of Methanol Synthesis from H2 and CO2 with Intermediate Condensation Steps, Processes 10 (2022) 1535, https://doi.org/10.3390/pr10081535.

[19] B.L. Campos, O. de, A.O.S. Costa, K.H. da, Delgado, S. Pitter, J. Sauer, E.F. Junior, C. da, Development of a surrogate artificial neural network for microkinetic modeling: case study with methanol synthesis, React. Chem. & Eng. 9 (2024) 1047–1060, https://doi.org/10.1039/D3RE00409K.

[20] O. Campos BL de, K.H. Delgado, S. Wild, F. Studt, S. Pitter, J. Sauer, Surface reaction kinetics of the methanol synthesis and the water gas shift reaction on Cu/ZnO/Al 2 O 3, React. Chem. & Eng. 6 (2021) 868–887, https://doi.org/10.1039/D1RE00040C.

[21] J. Pfersich, P.J. Arauzo, M. Lucian, P. Modugno, M.-M. Titirici, L. Fiori, et al., Hydrothermal Conversion of Spent Sugar Beets into High-Value Platform Molecules, Molecules 25 (2020) 3914, https://doi.org/10.3390/molecules25173914.

[22] Y. Tachibana, K. Kasuya, Chapter 10 - Bio-based polymers synthesized from furan derivatives, in: V. Sessini, S. Ghosh, M.E.G. Mosquera (Eds.), Biopolymers, Elsevier, 2023, pp. 295–345, https://doi.org/10.1016/B978-0-323-90939-6.00011-X.

[23] A. Gandini, T. M. Lacerda, Furan Polymers: State of the Art and Perspectives, Macromol. Mater. Eng. 307 (2022) 2100902, https://doi.org/10.1002/mame.202100902.

[24] A. Lourenço, H. Pereira, A. Lourenço, H. Pereira, Compositional Variability of Lignin in Biomass. Lignin - Trends and Applications, IntechOpen, 2017, https://doi.org/10.5772/intechopen.71208.

[25] A. Bresinsky, C. Körner, J.W. Kadereit, G. Neuhaus, U. Sonnewald, Lehrbuch der Botanik. 36. Aufl, Spektrum Akad. Verl, Heidelberg, 2008 (https://doi.org/Eduard).

[26] H. Lange, S. Decina, C. Crestini, Oxidative upgrade of lignin – Recent routes reviewed, Eur. Polym. J. 49 (2013) 1151–1173, https://doi.org/10.1016/j.eurpolymj.2013.03.002.

[27] F. José Borges Gomes, R.E. Souza, E.O. Brito, R.C. Costa Lelis, A review on lignin sources and uses, JABB (2020) 100–105, https://doi.org/10.15406/jabb.2020.07.00222.

[28] Metsä Group. Metsä Group. Sustainability Report 2018. 2019.

[29] J. Clark, F. Deswarte, The Biorefinery Concept, in: J.H. Clark, F.E.I. Deswarte (Eds.), Introduction to chemicals from biomass, Wiley, Chichester, West Sussex, 2015, pp. 1–29, https://doi.org/10.1002/9781118714478.ch1.

[30] A.F. Ferreira, Biorefinery Concept, in: M. Rabaçal, A.F. Ferreira, C.A.M. Silva, M. Costa (Eds.), Bio-refineries: Targeting energy, high value products and waste valorisation, vol, 57, Springer, Cham, 2017, pp. 1–20, https://doi.org/10.1007/978-3-319-48288-0_1.

[31] M. Rabaçal, A.F. Ferreira, C.A.M. Silva, M. Costa, Bio-refineries: Targeting, in: energy, high value products and waste valorisation, 57, Springer, Cham, 2017 (https://doi.org/Miriam).

[32] A.J. Ragauskas, C.K. Williams, B.H. Davison, G. Britovsek, J. Cairney, C.A. Eckert, et al., The path forward for biofuels and biomaterials, Science 311 (2006) 484–489, https://doi.org/10.1126/science.1114736.

[33] F. Cherubini, The biorefinery concept: Using biomass instead of oil for producing energy and chemicals, Energy Convers. Manag. 51 (2010) 1412–1421, https://doi.org/10.1016/j.enconman.2010.01.015.

[34] Äänekoski bioproduct mill Brochure EN n.d. ⟨https://materialsmetsafibre.metsagroup.com/view/1035841001?sharedOn⟩= (accessed January 4, 2025).

[35] Lenzing – von Natur innovativ 2025. ⟨https://www.lenzing.com/de/⟩ (accessed November 9, 2025).

[36] Bioraffinerie Leuna. Bioraffinerie Leuna | UPM Biochemicals 2025. ⟨https://www.upmbiochemicals.com/de/uber-upm-biochemicals/bioraffinerie-leuna/⟩ (accessed November 9, 2025).

[37] D. Rodríguez-Escribano, F. de Salas, R. Pliego, G. Marques, T. Levée, A. Suonpää, et al., Depolymerisation of Kraft Lignin by Tailor-Made Alkaliphilic Fungal Laccases, Polymers 15 (2023) 4433, https://doi.org/10.3390/polym15224433.

[38] C. Weng, X. Peng, Y. Han, Depolymerization and conversion of lignin to value-added bioproducts by microbial and enzymatic catalysis, Biotechnol. Biofuels 14 (2021) 84, https://doi.org/10.1186/s13068-021-01934-w.

[39] A. Leonowicz, N. Cho, J. Luterek, A. Wilkolazka, M. Wojtas-Wasilewska, A. Matuszewska, et al., Fungal laccase: properties and activity on lignin, J. Basic Microbiol. 41 (2001) 185–227, https://doi.org/10.1002/1521-4028(200107)41:3/4%253C185::AID-JOBM185%253E3.0.CO;2-T.

[40] O. Movil-Cabrera, A. Rodriguez-Silva, C. Arroyo-Torres, J.A. Staser, Electrochemical conversion of lignin to useful chemicals, Biomass.. Bioenergy 88 (2016) 89–96, https://doi.org/10.1016/j.biombioe.2016.03.014.

[41] B. Xie, Y. Tobimatsu, K. Narita, S. Yokohata, H. Kamitakahara, T. Takano, Electro-Oxidation of Lignin Model Compounds and Synthetic Lignin with Transition-Metal Complexes (Manganese and Iron Complexes), ACS Sustain. Chem. Eng. 10 (2022) 16701–16708, https://doi.org/10.1021/acssuschemeng.2c04811.

[42] D.D. Marino, V. Aniko, A. Stocco, S. Kriescher, M. Wessling, Emulsion electro-oxidation of kraft lignin, Green. Chem. 19 (2017) 4778–4784, https://doi.org/10.1039/C7GC02115A.

[43] E. Paone, A. Beneduci, G.A. Corrente, A. Malara, F. Mauriello, Hydrogenolysis of aromatic ethers under lignin-first conditions, Mol. Catal. 497 (2020) 111228, https://doi.org/10.1016/j.mcat.2020.111228.

[44] L. Hdidou, L. Kouisni, B. Manoun, H. Hannache, A. Solhy, A. Barakat, Oxidative conversion of lignin over cobalt-iron mixed oxides prepared via the alginate gelation, Catal. Commun. 117 (2018) 99–104, https://doi.org/10.1016/j.catcom.2018.08.027.

[45] L. Hdidou, K. Khallouk, A. Solhy, B. Manoun, A. Oukarroum, A. Barakat, Synthesis of CoFeO mixed oxides via an alginate gelation process as efficient heterogeneous catalysts for lignin depolymerization in water, Catal. Sci. Technol. 8 (2018) 5445–5453, https://doi.org/10.1039/C8CY00576A.

[46] J. Mottweiler, T. Rinesch, C. Besson, J. Buendia, C. Bolm, Iron-catalysed oxidative cleavage of lignin and β-O-4 lignin model compounds with peroxides in DMSO, Green. Chem. 17 (2015) 5001–5008, https://doi.org/10.1039/C5GC01306B.

[47] X. Huang, C. Atay, T.I. Korányi, M.D. Boot, E.J.M. Hensen, Role of Cu–Mg–Al Mixed Oxide Catalysts in Lignin Depolymerization in Supercritical Ethanol, ACS Catal. 5 (2015) 7359–7370, https://doi.org/10.1021/acscatal.5b02230.

[48] M.R. Sturgeon, S. Kim, K. Lawrence, R.S. Paton, S.C. Chmely, M. Nimlos, et al., A Mechanistic Investigation of Acid-Catalyzed Cleavage of Aryl-Ether Linkages: Implications for Lignin Depolymerization in Acidic Environments, ACS Sustain. Chem. Eng. 2 (2014) 472–485, https://doi.org/10.1021/sc400384w.

[49] X. Erdocia, R. Prado, M.Á. Corcuera, J. Labidi, Base catalyzed depolymerization of lignin: Influence of organosolv lignin nature, Biomass.. Bioenergy 66 (2014) 379–386, https://doi.org/10.1016/j.biombioe.2014.03.021.

[50] A. Kruse, N. Dahmen, Water – A magic solvent for biomass conversion, J. Supercrit. Fluids 96 (2015) 36–45, https://doi.org/10.1016/j.supflu.2014.09.038.

[51] S.E. Hunter, P.E. Savage, Recent advances in acid- and base-catalyzed organic synthesis in high-temperature liquid water, Chem. Eng. Sci. 59 (2004) 4903–4909, https://doi.org/10.1016/j.ces.2004.09.009.

[52] N. Akiya, P.E. Savage, Roles of water for chemical reactions in high-temperature water, Chem. Rev. 102 (2002) 2725–2750, https://doi.org/10.1021/cr000668w.

[53] T. Belkheiri, S.-I. Andersson, C. Mattsson, L. Olausson, H. Theliander, L. Vamling, Hydrothermal liquefaction of kraft lignin in sub-critical water: the influence of the sodium and potassium fraction, Biomass.. Conv. Bioref. 8 (2018) 585–595, https://doi.org/10.1007/s13399-018-0307-9.

[54] T. Belkheiri, S.-I. Andersson, C. Mattsson, L. Olausson, H. Theliander, L. Vamling, Hydrothermal Liquefaction of Kraft Lignin in Subcritical Water: Influence of Phenol as Capping Agent, Energy Fuels 32 (2018) 5923–5932, https://doi.org/10.1021/acs.energyfuels.8b00068.

[55] S. Cheng, C. Wilks, Z. Yuan, M. Leitch, C. Xu, Hydrothermal degradation of alkali lignin to bio-phenolic compounds in sub/supercritical ethanol and water–ethanol co-solvent, Polym. Degrad. Stab. 97 (2012) 839–848, https://doi.org/10.1016/j.polymdegradstab.2012.03.044.

[56] D. Forchheim, U. Hornung, A. Kruse, T. Sutter, Kinetic Modelling of Hydrothermal Lignin Depolymerisation, Waste Biomass.. Valor 5 (2014) 985–994, https://doi.org/10.1007/s12649-014-9307-6.
[57] J.R. Gasson, D. Forchheim, T. Sutter, U. Hornung, A. Kruse, T. Barth, Modeling the Lignin Degradation Kinetics in an Ethanol/Formic Acid Solvolysis Approach. Part 1. Kinetic Model Development, Ind. Eng. Chem. Res 51 (2012) 10595–10606, https://doi.org/10.1021/ie301487v.
[58] A. Toledano, L. Serrano, J. Labidi, Improving base catalyzed lignin depolymerization by avoiding lignin repolymerization, Fuel 116 (2014) 617–624, https://doi.org/10.1016/j.fuel.2013.08.071.
[59] A. Ahlbom, M. Maschietti, R. Nielsen, M. Hasani, H. Theliander, Using guaiacol as a capping agent in the hydrothermal depolymerisation of kraft lignin, Nord. Pulp & Pap. Res. J. 38 (2023) 619–631, https://doi.org/10.1515/npprj-2023-0013.
[60] A. Ahlbom, M. Maschietti, R. Nielsen, H. Lyckeskog, M. Hasani, H. Theliander, Using Isopropanol as a Capping Agent in the Hydrothermal Liquefaction of Kraft Lignin in Near-Critical Water, Energies 14 (2021) 932, https://doi.org/10.3390/en14040932.
[61] A. Ahlbom, M. Maschietti, R. Nielsen, M. Hasani, H. Theliander, On the hydrothermal depolymerisation of kraft lignin using glycerol as a capping agent, Holzforschung 77 (2023) 159–169, https://doi.org/10.1515/hf-2022-0146.
[62] D. Forchheim, U. Hornung, P. Kempe, A. Kruse, D. Steinbach, Influence of RANEY Nickel on the Formation of Intermediates in the Degradation of Lignin, Int. J. Chem. Eng. 2012 (2012) 1–8, https://doi.org/10.1155/2012/589749.
[63] S. Harisankar, R. Vinu, Platform chemicals from hardwood black liquor via hydrothermal liquefaction: influence of process conditions on product yields and quality, Sustain. Energy & Fuels 7 (2023) 4423–4441, https://doi.org/10.1039/D3SE00308F.
[64] M. Huet, A. Roubaud, C. Chirat, D. Lachenal, Hydrothermal treatment of black liquor for energy and phenolic platform molecules recovery in a pulp mill, Biomass.. Bioenergy 89 (2016) 105–112, https://doi.org/10.1016/j.biombioe.2016.03.023.
[65] M. Wörner, A. Barsuhn, T. Zevaco, U. Hornung, N. Dahmen, From Pulp to Aromatic Products - Reaction Pathways of Lignin Depolymerization, Energy Fuels (2024), https://doi.org/10.1021/acs.energyfuels.3c04509.
[66] M. Jayathilake, S. Rudra, L.A. Rosendahl, Hydrothermal liquefaction of wood using a modified multistage shrinking-core model, Fuel 280 (2020) 118616, https://doi.org/10.1016/j.fuel.2020.118616.
[67] T.L.-K. Yong, Y. Matsumura, Reaction Kinetics of the Lignin Conversion in Supercritical Water, Ind. Eng. Chem. Res 51 (2012) 11975–11988, https://doi.org/10.1021/ie300921d.
[68] T.L.-K. Yong, Y. Matsumura, Kinetic Analysis of Lignin Hydrothermal Conversion in Sub- and Supercritical Water, Ind. Eng. Chem. Res 52 (2013) 5626–5639, https://doi.org/10.1021/ie400600x.
[69] M. Cardoso, É.D. Oliveira, M.L. Passos, Chemical composition and physical properties of black liquors and their effects on liquor recovery operation in Brazilian pulp mills, Fuel 88 (2009) 756–763, https://doi.org/10.1016/j.fuel.2008.10.016.
[70] M. Wörner, L. Werner, N.I. Canabarro, D. Baudouin, U. Hornung, N. Dahmen, The Impact of Sulfur-containing Inorganic Compounds during the Depolymerization of Lignin by Hydrothermal Liquefaction of Black Liquor, Energy Fuels (2024), https://doi.org/10.1021/acs.energyfuels.3c04737.
[71] Wahyudiono, M. Sasaki, M. Goto, Conversion of biomass model compound under hydrothermal conditions using batch reactor, Fuel 88 (2009) 1656–1664, https://doi.org/10.1016/j.fuel.2009.02.028.
[72] Wahyudiono, M. Sasaki, M. Goto, Thermal decomposition of guaiacol in sub- and supercritical water and its kinetic analysis, J. Mater. Cycles Waste Manag 13 (2011) 68–79, https://doi.org/10.1007/s10163-010-0309-6.
[73] S.F. Hashmi, H. Meriö-Talvio, K.J. Hakonen, K. Ruuttunen, H. Sixta, Hydrothermolysis of organosolv lignin for the production of bio-oil rich in monoaromatic phenolic compounds, Fuel Process. Technol. 168 (2017) 74–83, https://doi.org/10.1016/j.fuproc.2017.09.005.
[74] Z. Pan, X. Wu, A. Bodi, J.A. van Bokhoven, P. Hemberger, Catalytic pyrolysis mechanism of lignin moieties driven by aldehyde, hydroxyl, methoxy, and allyl functionalization: the role of reactive quinone methide and ketene intermediates, Green. Chem. 26 (2024) 9899–9910, https://doi.org/10.1039/D4GC03143A.
[75] N. Boukis, V. Diem, W. Habicht, E. Dinjus, Methanol Reforming in Supercritical Water, Ind. Eng. Chem. Res 42 (2003) 728–735, https://doi.org/10.1021/ie020557i.
[76] Wahyudiono, M. Sasaki, M. Goto, Recovery of phenolic compounds through the decomposition of lignin in near and supercritical water, Chem. Eng. Process. Process.Intensif. 47 (2008) 1609–1619, https://doi.org/10.1016/j.cep.2007.09.001.
[77] C.L. Yaws. The Yaws handbook of vapor pressure: Antoine coefficients, 2nd edition., Elsevier/GPP, Gulf Professional Publishing is an imprint of Elsevier, Amsterdam Boston, 2015.
[78] G. James, D. Witten, T. Hastie, R. Tibshirani, An Introduction to Statistical Learning: with Applications in R. Zweite Ausgabe 2021 Edition, Springer, New York, 2021.
[79] Y. Slotboom, M.J. Bos, J. Pieper, V. Vrieswijk, B. Likozar, S.R.A. Kersten, et al., Critical assessment of steady-state kinetic models for the synthesis of methanol over an industrial Cu/ZnO/Al2O3 catalyst, Chem. Eng. J. 389 (2020) 124181, https://doi.org/10.1016/j.cej.2020.124181.
[80] G. Rodrigues Niquini, B. Lacerda de Oliveira Campos, K. Herrera Delgado, S. Pitter, J. Sauer, Experimental study and comprehensive kinetic modeling of the direct dimethyl ether synthesis on Cu/ZnO/ZrO2 and H-FER-20, Chem. Eng. J. 480 (2024) 147968, https://doi.org/10.1016/j.cej.2023.147968.
[81] C. Wang, Y. Fan, U. Hornung, W. Zhu, N. Dahmen, Char and tar formation during hydrothermal treatment of sewage sludge in subcritical and supercritical water: Effect of organic matter composition and experiments with model compounds, J. Clean. Prod. 242 (2020) 118586, https://doi.org/10.1016/j.jclepro.2019.118586.
[82] J. Towfighi, M. Sadrameli, A. Niaei, Coke Formation Mechanisms and Coke Inhibiting Methods in Pyrolysis Furnaces, J. Chem. Eng. Jpn. / JCEJ 35 (2002) 923–937, https://doi.org/10.1252/jcej.35.923.
[83] A. Kruse, D. Meier, P. Rimbrecht, M. Schacht, Gasification of Pyrocatechol in Supercritical Water in the Presence of Potassium Hydroxide, Ind. Eng. Chem. Res 39 (2000) 4842–4848, https://doi.org/10.1021/ie0001570.
[84] H. Yang, W. Yin, X. Zhu, P.J. Deuss, H.J. Heeres, Selective Demethoxylation of Guaiacols to Phenols using Supported MoO3 Catalysts, ChemCatChem 14 (2022) e202200297, https://doi.org/10.1002/cctc.202200297.
[85] M. Ishikawa, M. Tamura, Y. Nakagawa, K. Tomishige, Demethoxylation of guaiacol and methoxybenzenes over carbon-supported Ru–Mn catalyst, Appl. Catal. B Environ. 182 (2016) 193–203, https://doi.org/10.1016/j.apcatb.2015.09.021.
[86] X. Ren, Q. Qiang, Z. Sun, T. Wei, X. Yu, Z. Rong, et al., Water Splitting Integrated with Self-Transfer Hydrogenolysis for Efficient Demethoxylation of Guaiacols to Phenols over the Ni/MgO Catalyst, ACS Catal. 14 (2024) 5247–5259, https://doi.org/10.1021/acscatal.4c00038.
[87] J. Schuler, U. Hornung, A. Kruse, N. Dahmen, J. Sauer, Hydrothermal Liquefaction of Lignin, JBNB 08 (2017) 96–108, https://doi.org/10.4236/jbnb.2017.81007.
[88] J. Schuler, U. Hornung, N. Dahmen, J. Sauer, Lignin from bark as a resource for aromatics production by hydrothermal liquefaction, GCB Bioenergy 11 (2019) 218–229, https://doi.org/10.1111/gcbb.12562.
[89] Schuler J. Hydrothermal liquefaction of lignin. Karlsruhe; 2020. https://doi.org/10.5445/IR/1000117444.
[90] N. Abad-Fernández, E. Pérez, M.J. Cocero, Aromatics from lignin through ultrafast reactions in water, Green. Chem. 21 (2019) 1351–1360, https://doi.org/10.1039/C8GC03989E.
[91] N. Abad-Fernández, E. Pérez, Á. Martín, M.J. Cocero, Kraft lignin depolymerisation in sub- and supercritical water using ultrafast continuous reactors. Optimization and reaction kinetics, J. Supercrit. Fluids 165 (2020) 104940, https://doi.org/10.1016/j.supflu.2020.104940.